

ABSTRACT

Title of Document: A NON-LINEAR DAMAGE MODEL WITH
LOAD DEPENDENT EXPONENTS FOR
SOLDERS UNDER SEQUENTIAL CYCLIC
SHEAR LOADS

Elviz George, Ph.D., 2015

Directed By: Professor Michael G. Pecht, Department of
Mechanical Engineering

The damage state of a material subject to cyclic loads is often characterized by the cycle ratio of applied cycles to the number of survivable cycles. The damage in a material under sequential cyclic loading is widely estimated using Miner's rule. Miner's rule assumes that damage in a material accumulates linearly under cyclic loading and the damage path is independent of the applied load level. Due to these inherent assumptions, Miner's rule inaccurately estimates life under sequential loading conditions for solders. To improve the accuracy of damage estimation, a non-linear damage accumulation model based on damage curve approach that takes into account the effect of loading sequence under sequential loading conditions is proposed for solders in this dissertation. In the proposed non-linear damage model, damage is related to the cycle ratio using a power law relationship where the power

law (damage) exponent is defined as a function of the applied load level (cycles to failure).

An experimental approach is proposed to determine the load dependent exponents of the non-linear model under three load levels. The test matrix consisted of a series of single level cyclic and sequential cyclic shear tests in a thermo-mechanical micro analyzer. Load dependent exponents were developed for SAC305 (96.5%Sn+3.0%Ag+0.5Cu) solder material and the applicability of these exponents were validated by tests under a new loading condition and reverse loading sequence. Experimental results revealed that the value of damage exponent decreased with the severity of the applied load level. Additionally, taking damage analogous to crack growth, an analytical relationship between the damage exponent and the applied load level was developed from the Paris' law for crack propagation. This enables determination of non-linear damage curves at different load levels without conducting extensive experimentation. The damage due to crack initiation was assumed to be 10% of the total damage and sensitivity analysis was carried out to determine the effect of this assumption. The load dependence of the Paris' law exponent (m) was also derived for SAC305 solder material. Analysis of the failed specimens revealed fatigue crack in the solder joints along the tin grain boundaries.

A NON-LINEAR DAMAGE MODEL WITH LOAD DEPENDENT EXPONENTS
FOR SOLDERS UNDER SEQUENTIAL CYCLIC SHEAR LOADS

By

Elviz George

Dissertation submitted to the Faculty of the Graduate School of the
University of Maryland, College Park, in partial fulfillment
of the requirements for the degree of
Doctor of Philosophy
2015

Advisory Committee:
Professor Michael Pecht, Chair
Professor Abhijit Dasgupta
Professor Patrick McCluskey
Professor Michael Ohadi
Professor David Barbe
Senior Research Scientist Dr. Michael Osterman

© Copyright by
Elviz George
2015

Dedication

I would like to dedicate my Ph.D. dissertation to my father, Dr. Zachariah Lakaparampil, and my mother, Mrs. Rosamma Jacob, both of whom have relentlessly encouraged me to pursue my career dreams since childhood. Further, I would like to dedicate my doctoral degree to my beloved wife, Dr. Chino Mannikarottu, who has constantly been by my side while I was going through the challenges of my research work. I would also like to dedicate my degree to my newborn angel, Ezri Laka George.

Acknowledgements

First and foremost, I would like to express my sincere appreciation to my advisor Prof. Michael Pecht, who has been a tremendous mentor for me and without whom this dissertation would have been impossible. Further, during my time here at the Center for Advanced Life Cycle Engineering (CALCE), there have been several people who allowed me to grow as a researcher; most important among them would be Dr. Michael Osterman and Prof. Abhijit Dasgupta. Your advice for my research process has been priceless and I would like to express my sincere gratitude to both of you. I would also like to thank Dr. Diganta Das for his insightful career advice.

In addition, my committee members for this thesis defense - Prof. Patrick McCluskey, Prof. Michael Ohadi and Prof. David Barbe have been kind enough for being part of my dissertation committee while providing me with brilliant comments and suggestions. Thank you to all of you.

My life as a research associate would not have been possible without the constant support from my family, which includes my parents and brother back in India, my in-laws, sister, wife and our newborn baby girl. Words cannot express my gratitude for all of the sacrifices that they all have made on my behalf. During the very demanding phase of my research, my friends and colleagues here at CALCE has supported me and encouraged me constantly to strive toward my goal. I would like to thank Sandeep Menon, Anto Peter, Dr. Carlos Morillo, Arvind Vasan, Sony Mathew, Bhanu Sood, Giovanni Flores, and Dengyun Chen from the bottom of my heart. I would also like to thank Qian Jiang for all the help and support in conducting tests in the thermo-mechanical micro analyzer test setup. Finally, I would like to thank God

for helping me get through my educational career and to keep my enthusiasm going to make my dream possible.

Table of Contents

Dedication	ii
Acknowledgements	iii
Table of Contents	v
List of Tables	vii
List of Figures	viii
Chapter 1: Introduction	1
Chapter 2: Literature Review	6
2.1. Concurrent loading.....	6
2.2. Sequential loading.....	7
2.2.1. Applicability of linear damage rule under sequential loading	8
2.2.2. Non-linear damage evolution under a single loading condition	12
2.2.3. Existing non-linear damage models for solder interconnects under sequential loading	16
2.2.4. Existing non-linear damage models for metals under sequential loading	28
2.3. Mapping of damage under different loading conditions.....	32
2.4. Gaps in existing research	34
2.5. Dissertation objectives	36
Chapter 3: Development of a Load Dependent Non-linear Damage Model for Sequential Loading	38
3.1. Load dependent non-linear damage model	38
3.2. Experimental approach to create damage curves.....	43
3.2.1. Determination of damage exponents	44
3.2.2. Damage exponent vs load level relationship	47
3.2.3. Damage mapping between load levels and load types.....	48
3.2.3. Assumptions/limitations of the approach.....	51
Chapter 4: Experimental Setup	53
4.1 Test specimen.....	55

4.2	Test profiles	58
4.3	Interpretation of raw data.....	61
Chapter 5: Load-dependent Non-Linear Damage Model		68
5.1	Derivation of the form of non-linear damage model	68
5.2	Development of damage curves at different load levels.....	71
5.3	Validation of non-linear model.....	73
5.3.1	Validation of damage exponents (under new loading condition)	74
5.3.2	Validation of damage exponents (under reverse load sequence).....	75
5.4	Relationship between damage exponent and applied load level.....	76
5.5	Physical explanation of damage curve model.....	79
5.6	Miner's rule vs non-linear damage model	84
5.7	Limitations of the non-linear damage model	85
Chapter 6: Dissertation Contributions		88
Chapter 7: Future Work		89
APPENDIX A: Analytical Relation from Experimental Fit.....		91
APPENDIX B: Failure Analysis.....		92
APPENDIX C: Load Drop for Load Levels 1, 2, and 3		93
APPENDIX D: Sensitivity of Failure Criterion.....		95
Bibliography		96

List of Tables

Table I. Cycles to failure for single step test conditions.....	18
Table II. Cumulative damage using Miner’s rule for T-V load sequence.	19
Table III. Cumulative damage using Miner’s rule for V-T load sequence.	19
Table IV. Exponents developed by Perkins for T-V sequence.....	20
Table V. Exponents developed by Perkins for V-T sequence.	21
Table VI. Exponents determined by Perkins	21
Table VII. Comparison of cumulative damage in T-V sequence using damage exponents developed using the maximum likelihood approach and by Perkins	23
Table VIII. Comparison of cumulative damage in V-T sequence using damage exponents developed using the maximum likelihood approach and by Perkins (first 2 cases omitted by Perkins were omitted in the maximum likelihood approach).	24
Table IX. Comparison of cumulative damage in V-T sequence using damage exponents developed using the maximum likelihood approach and by Perkins (first 2 cases omitted by Perkins were not omitted in the maximum likelihood approach). ..	25
Table X. Exponents determined from the maximum likelihood approach.....	26
Table XI. Test profiles.....	59
Table XII. Comparison of non-linear model and Miner’s rule predictions to experimental results under new loading condition.	74
Table XIII. Comparison of non-linear model and Miner’s rule predictions to experimental results under reverse loading sequence.....	75
Table XIV. Sensitivity of damage exponents to the change in percentage initiation.	79
Table XV. Coefficients from experimental data.....	91
Table XVI. Sensitivity of percentage load drop on the developed damage exponents	95

List of Figures

Figure 1. Crack propagation in solders under cyclic loading	2
Figure 2. Miner's linear damage rule	4
Figure 3. Multiple loads in electronic assemblies.....	4
Figure 4. Damage under concurrent and sequential loading conditions.....	5
Figure 5. Crack propagation of SAC105 solder under low-high and high-low amplitude testing [17]	9
Figure 6. Sequence independence in Miner's rule [17].....	9
Figure 7. Error in Miner's rule prediction compared to experimental results under sequential loading conditions [18].....	10
Figure 8. Damage estimation using Miner's rule under T-V and V-T load sequences [19].....	11
Figure 9. Damage function by Wen et al. [21]	13
Figure 10. Plot of (a) η_p and (b) η_c for different values of inelastic strain ranges [20]	15
Figure 11. Comparison of experimental and model data [22]	16
Figure 12. Non-linear fit by Perkins and Sitaraman	22
Figure 13. Hardness as a potential damage parameter.....	27
Figure 14. Marco and Starkey approach.....	29
Figure 15. Non-linear damage curves by Manson and Halford.....	31
Figure 16. Schematic of damage mapping between isothermal aging and temperature cycling [23]	33
Figure 17. Damage mapping between isothermal aging and temperature cycling using phase growth model [23]	34
Figure 18. Dependence of damage exponent on strain range (adapted from [20]).....	36
Figure 19. Damage curve at different life/load levels.....	39
Figure 20. Effect of load sequence in a non-linear damage model under a harsh-mild load sequence	40
Figure 21. Effect of load sequence in a non-linear damage model under mild-harsh load sequence	41

Figure 22. Simulation of cycle counts under a harsh-mild loading condition	42
Figure 23. Simulation of damage propagation under a harsh-mild loading condition	43
Figure 24. Experimental approach to develop damage curves	44
Figure 25. Determination of damage exponents from two sets of sequential tests.....	45
Figure 26. Experimental suite to determine damage curves at three load levels.....	47
Figure 27. Dependence of damage exponents on load levels and life	48
Figure 28. Damage mapping for different load levels	50
Figure 29. Damage mapping for different load types	51
Figure 30. Damage distributions.....	52
Figure 31 (a) TMM test setup	53
Figure 32. Input and output of the proposed non-linear damage model	55
Figure 33. TMM test specimen.....	56
Figure 34. TMM test specimen schematic.....	56
Figure 35. Shear stress distribution in a TMM test specimen [29].....	56
Figure 36. (a) specimen attached to the specimen grips (b) schematic of specimen in grips (red arrow shows the direction of motion of the movable grip)	58
Figure 37. S-N durability curves for SAC solder [30].....	59
Figure 38. Adaptive inelastic strain range (ISR) controlled testing process including cycle update criterion and adjustment calculation (maximum and minimum amplitudes) [28].....	60
Figure 39. Solder joint height measurements	62
Figure 40. Effect of taper on shear stress and shear strain [29].....	63
Figure 41. Baseline cycle for the case of load level 3	64
Figure 42. Hysteresis loop during inelastic strain range controlled cyclic test (load level 3)	65
Figure 43. Drop in load during constant inelastic strain range controlled test (load level 3).	66
Figure 44. Inelastic strain range during test.....	67
Figure 45. Average cycles to failure under different test profiles.	72
Figure 46. Damage curves for load levels 1, 2, and 3.....	73

Figure 47. Relationship between Paris' law exponent (m) and cycles of failure of the applied load level	77
Figure 48. Relationship between Paris' law exponent (m) and cycles of failure of the applied load level	78
Figure 49. Lattice approximation of a polycrystalline material [33]	80
Figure 50. Failure site in a test specimen subjected to load level 1 followed by load level 3 until failure	82
Figure 51. Tin grains in untested SAC solder specimen.....	83
Figure 52. Crack propagation along the tin grain boundary	84
Figure 53. Relationship between damage exponent and cycles to failure.	91
Figure 54. Failure site in a test specimen subjected to load level 2 until failure	92
Figure 55. Failure site in a test specimen subjected to load level 1 until failure	92
Figure 56. Average load drop under load level 1 (bounds = one standard deviation)	93
Figure 57. Average load drop under load level 2 (bounds = one standard deviation)	93
Figure 58. Average load drop under load level 3 (bounds = one standard deviation)	94
Figure 59. Damage exponents with a failure criterion of 70% load drop.....	95

Chapter 1: Introduction

Solder joints provide mechanical, electrical, and thermal connections between packaged electronic devices and the printed circuit board in electronics assemblies. In use, solder joints are subjected to loading conditions that over time may result in their failure. One of the most common loading conditions is temperature excursion. Temperature excursions can occur due to heat generated during operation and changes in ambient temperature as part of the diurnal cycle. Because of the variations in temperature expansion of materials used in the construction of the packaged device and board, temperature excursions can result in thermo-mechanical stresses in solder joints. Under repeated temperature excursions, thermo-mechanical stresses can cause fatigue-induced fracture over time (see Figure 1). The thermal cycling reliability of lead-based and lead-free solder interconnects has been studied extensively in the literature [1][2][3][4][5].

The requirement for higher performance and portability for mobile electronics has resulted in the development of smaller form factor, thinner and high density configuration packages. With the miniaturization of electronic packages and increased portability, the solder joints in mobile electronics are more susceptible to failure due to mechanical loads resulting from field conditions such as bend, vibration or drop. Mechanical durability of solder joints under mechanical bend [6], vibration [7], and drop [8] has also been studied in the literature. In general, one of the most dominant failure mechanism in solder interconnects is fatigue fracture due to cyclic loading conditions.

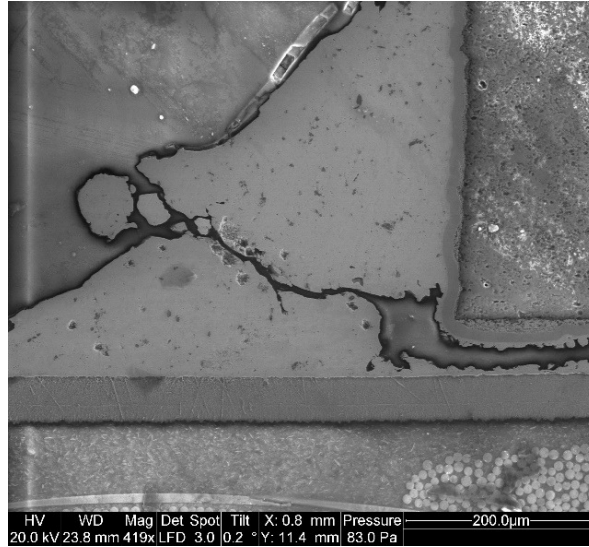


Figure 1. Crack propagation in solders under cyclic loading

One of the most widely used metrics to represent the health of solders is damage. Under a cyclic loading condition, damage is defined as the percentage of useful life removed from a system/component under the applied cyclic loading. Application of these cyclic loads results in fatigue of the material that may cause fracture over time. Mathematically, damage in cyclic loading is represented as a numerical value defined as a function of the ratio of applied number of cycles to the cycles to failure at a specific loading condition (see Equation 1).

Equation 1

$$D = \sum f(r_i) = \sum f\left(\frac{n_i}{N_{f_i}}\right)$$

where n is the applied number of cycles, N_f is the cycles to failure, and i is the loading condition.

Typically, the numerical value of damage is considered as 0 prior to the application of any cyclic loading and as unity when the solder interconnect has failed.

Various studies in literature have reported a critical damage parameter (D_c) with a numerical value lower than 1 for cases where the test is not continued until complete failure. Under multiple load conditions, damage is estimated as the summation of cycle ratio functions at each loading condition.

One of the earliest attempts to define damage function under cyclic loading in any material was by Palmgren [9] wherein it was suggested that the fatigue damage accumulates in a material linearly with use. Miner [10] mathematically represented the linear damage as defined in Equation 2. This concept originally proposed by Palmgren is graphically represented in Figure 2. According to Miner, damage is defined as the summation of the ratios of applied number of cycles to the cycles to failure at each loading condition (see Equation 2).

Equation 2

$$D = \sum r_i = \sum \frac{n_i}{N_{f_i}}$$

where n = applied number of cycles, N_f = cycles to failure, and i = loading condition.

In this relation, the failure of the system/component occurs when the numerical value of damage reaches unity. Since Miner's rule is dependent only on the applied number of cycles and cycles to failure, damage accumulation always follows a straight line (see Figure 2) regardless of the magnitude of the applied load level. Due to the linear nature and ease of implementation, Miner's rule has been widely used to represent damage in a variety of materials including solders.

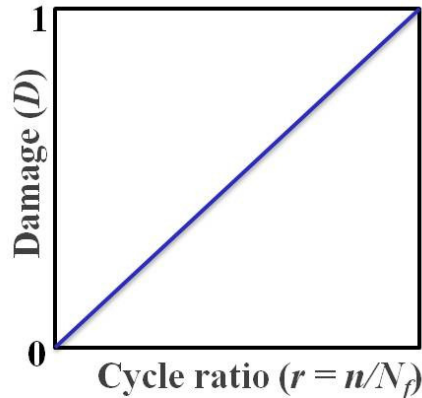


Figure 2. Miner's linear damage rule

A review of the existing literature revealed that the reliability of solder interconnects under single/single level cyclic thermal or mechanical loading conditions has been the primary focus and has been studied extensively [1][2][3][4][5][6][7][8]. However during manufacture and use, solder joints are often subjected to more than one load level or load type. These loads maybe applied concurrently (at the same time) or sequentially (one after the other) during use (see Figure 3).

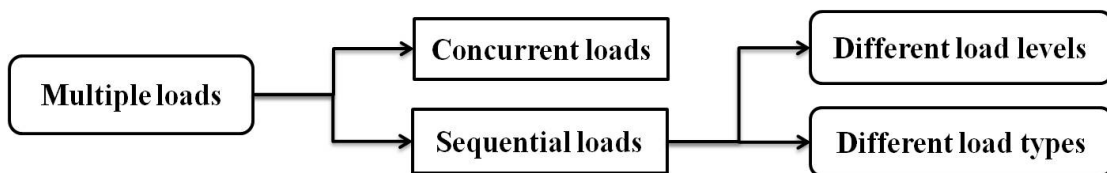


Figure 3. Multiple loads in electronic assemblies

For instance, before use the printed circuit assemblies (PCAs) would have already accumulated some level of damage from processing, transportation or preconditioning. During use, the PCAs may be subjected to loading conditions at different load levels (high-low or low-high). In addition to temperature excursions due to operation, mobile electronics may be subjected to mechanical loading during keypad presses, back-pocket crushing and handling.

For these cases of multiple loading conditions, damage models developed for single level cyclic loading conditions may not be applicable. For instance, can the damage accumulation be summed up using Miner's linear rule? Can the damage under individual load levels be superimposed to obtain the damage under multiple loading conditions (see Figure 4)? **Chapter 2: Literature Review** of this dissertation provides an overview of the existing literature on the damage accumulation methods under multiple loading conditions. Additionally, the research gaps in the existing literature and the objectives of this dissertation are also provided.

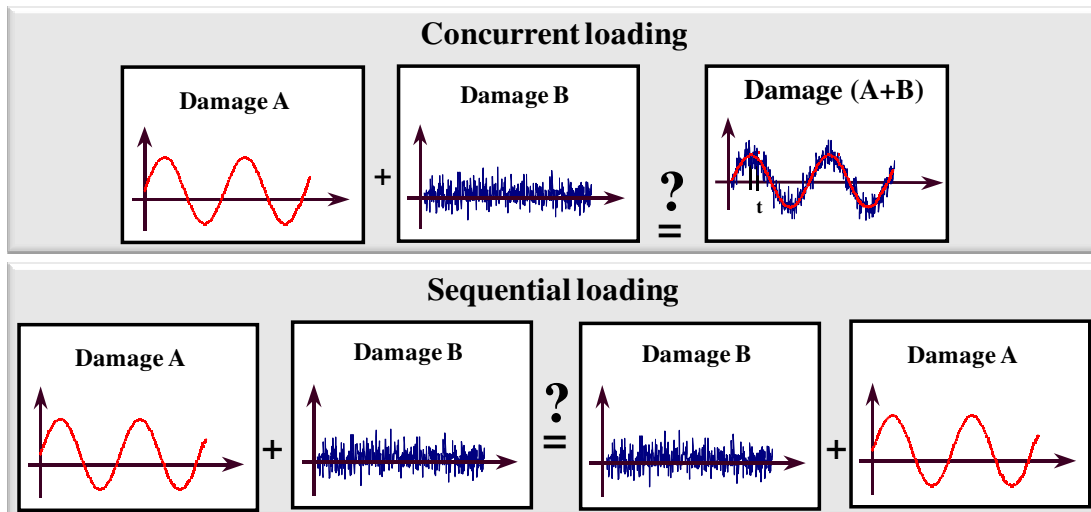


Figure 4. Damage under concurrent and sequential loading conditions

Chapter 2: Literature Review

The existing literature on the damage models for both multiple loading cases, i.e., concurrent loading and sequential loading, are discussed in this chapter. For both concurrent and sequential loading conditions, various studies in the literature have used Miner's linear rule as a first order approximation to estimate damage.

2.1. Concurrent loading

Concurrent loading is defined as the application of a loading condition along with another loading condition of a different load type. For concurrent loading conditions in solder interconnects, various lifetime estimation and modeling techniques have been proposed in the literature. Barker et al. [11] proposed a methodology to evaluate the combined effects of simultaneous thermal and vibration loads in solder interconnects. The effects of standalone thermal and vibration loads were superimposed to simulate the effects of combined loading conditions. Using Palmgren-Miner's linear superposition rule, the damage due to single level cyclic thermal and vibration loads were determined individually and superposed to obtain the effective solder joint life under combined loading conditions. Upadhyayula and Dasgupta [12] showed that Palmgren-Miner's linear superposition rule does not take into account the load interactions under combined thermal and vibration loading condition. Combined load effects were estimated using an incremental damage superposition approach (IDSA) that uses a variant of Miner's hypothesis, but in an incremental piece-wise linear sense for varying stress levels, to track nonlinear interactions between different load types (thermal cycling and vibration). Qi et al.

[13] showed that solder joints failed earlier under combined loading than with either separate temperature cycling or room temperature vibration loading. Qi also used IDSA proposed by Upadhyayula to accurately estimate the life expectancy of solder joints under combined temperature cycling and vibration loading. Yang et al. [14] imposed a cyclic out-of-plane deformation on a printed circuit board (PCB) assembly by twisting the PCB mechanically inside a thermal chamber. The fatigue life of the solder interconnections was predicted using Darveaux's crack initiation and growth model. Chen et al. [15] conducted cyclic four-point bend tests on soldered ball grid array packages executed at different controlled temperatures. Results showed that the component life cycle reduced with the increase in temperature. Montoya et al. [16] studied the reliability of leadless packages (capacitors and resistors) in a synchronized combined thermal and mechanical bending approach. The packages were subjected to mechanical strain of +/- 350, 750 and 1000 μ strain and temperature profile of -50°C to 150°C. The cycles to failure in their study reduced with the increase in mechanical strain.

2.2. Sequential loading

Sequential loading is defined as the application of a loading condition followed by another loading condition of a different load level or load type. The review of existing literature in sequential loading is broadly classified into three sections. In the first section, 2.2.1, the inaccuracies in the use of Miner's linear rule under sequential loading conditions are discussed. In section 2.2.2, the non-linear damage evolution models developed for solder interconnects under a single loading condition has been reviewed. In section 2.2.3, studies addressing the non-linear damage evolution in

solder interconnects under sequential loading conditions are presented. In section 2.2.4, studies addressing the non-linear damage evolution in other materials under sequential loading conditions are presented.

2.2.1. Applicability of linear damage rule under sequential loading

In this section, the applicability of Miner's linear rule under sequential loading of solder interconnects is discussed. For sequential cyclic loading of solder interconnects, the literature points to deficiencies with Miner's linear damage accumulation model.

A consortium of NXP, Freescale, ASE, and AStar-IME [17] conducted high speed cyclic bend test on modified ball grid array (BGA) packages using two-step loading to determine the applicability of Miner's rule. The PCB strain amplitudes were 1.2×10^{-3} and 1.8×10^{-3} for the low and high loading conditions. Damage accumulation was considered analogous to the percentage growth in crack length. Test results showed that Miner's rule was overly simplistic in the case of low-high amplitude loading conditions and resulted in the overestimation of fatigue life (see Figure 5).

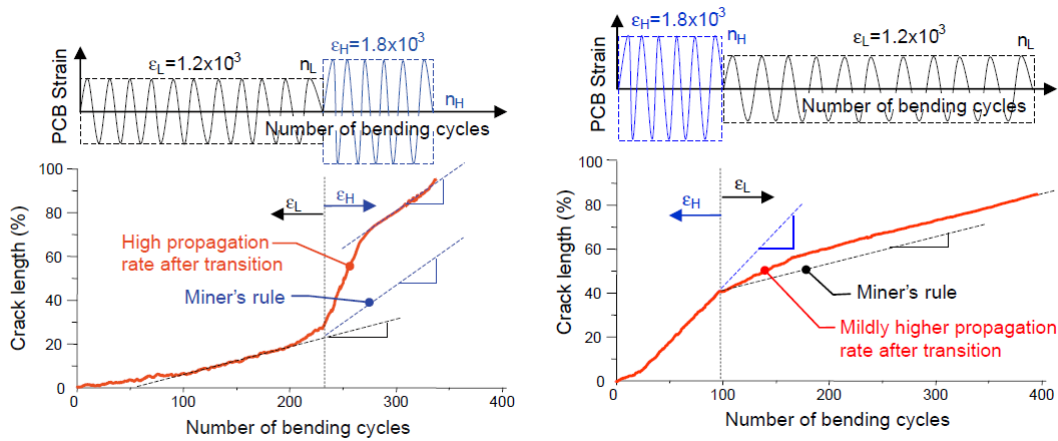


Figure 5. Crack propagation of SAC105 solder under low-high and high-low amplitude testing [17]

The principle of Miner's rule for a two-step loading is illustrated in Figure 6. Failure occurs when the total damage reaches unity regardless the path taken. Therefore, Miner's rule does not take into account the effect of sequence of load levels under sequential loading conditions.

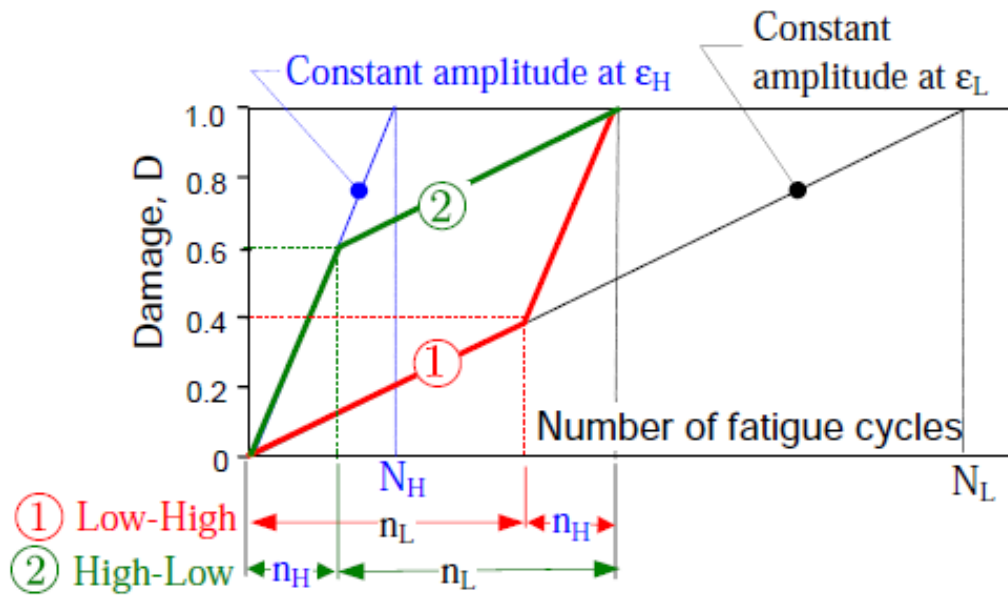


Figure 6. Sequence independence in Miner's rule [17]

Yang et al. [18] conducted shear fatigue testing of BGA components soldered using SAC305 and SAC405 alloys under harsh and mild loads. A systematic trend was observed where Miner's rule underestimated the life for loading sequences starting with mild cycling followed by harsh cycling. On the other hand, Miner's rule over-predicted the life for loading conditions starting with harsh cycling followed by mild cycling (see Figure 7).

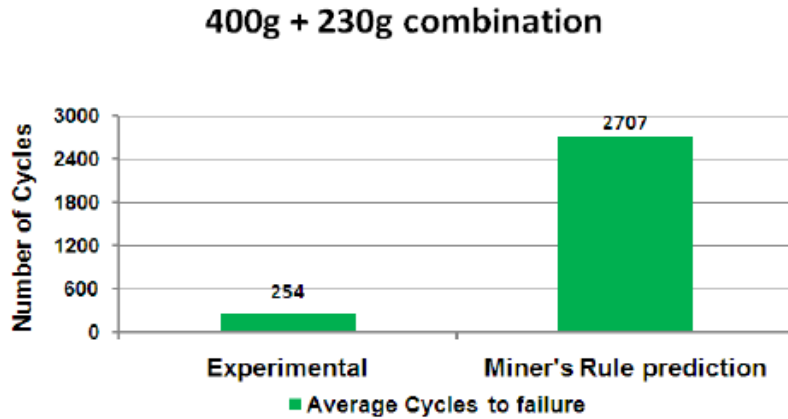


Figure 7. Error in Miner’s rule prediction compared to experimental results under sequential loading conditions [18]

Results from [17] [18] showed that Miner’s rule does not accurately consider the effect of sequence and stress levels under sequential loading of the same type. Perkins and Sitaraman [19] found that Miner’s rule was incapable of accounting for damage under a two-step temperature cycling and vibration sequential loading. Ceramic column grid array (CCGA) packages using a 90Pb10Sn solder column with eutectic tin lead solder fillets on both sides were subjected to four different types of experimental tests: 1) single step vibration alone to failure, 2) single step temperature cycling alone to failure, 3) two step loading T-V (temperature cycling for a specified time followed by vibration to solder joint failure), 4) and two step loading V-T (vibration for a specified time followed by temperature cycling to solder joint failure). Results show that for a T-V sequence, the use of Miner’s rule resulted in a damage value less than unity (0.66) whereas for a V-T sequence, the cumulative damage was close to unity (0.96) (see Figure 8). The discrepancy in the cumulative damage values when the sequence was reversed showed that Miner’s rule was incapable of accounting for the sequence effect. Therefore, a non-linear damage model based on a

power law was developed by the authors. The details of test conditions and non-linear model have been discussed in detail in section 2.2.3.

T-V Load Sequence				
n_1	n_1/N_1	n_2	n_2/N_2	Total Fatigue Life Ratio ($n_1/N_1 + n_2/N_2$)
800	0.50	6.93E4	0.04	0.54
800	0.50	1.15E5	0.06	0.57
800	0.50	1.35E5	0.07	0.58
800	0.50	2.86E5	0.16	0.66
800	0.50	3.38E5	0.19	0.69
800	0.50	8.94E5	0.49	0.99
800	0.50	9.84E5	0.54	1.04
Mean				0.73
Median				0.66
Range				0.50

V-T Load Sequence				
n_1	n_1/N_1	n_2	n_2/N_2	Total Fatigue Life Ratio ($n_1/N_1 + n_2/N_2$)
5.76E5	0.32	890	0.56	0.88
5.33E5	0.29	1000	0.63	0.92
5.40E5	0.30	1100	0.69	0.99
4.19E5	0.23	1300	0.82	1.05
Mean				0.96
Median				0.96
Range				0.17

Figure 8. Damage estimation using Miner’s rule under T-V and V-T load sequences [19]

From the review of the existing literature, it can be concluded that since Miner’s rule assumes a linear damage accumulation, the application of Miner’s linear damage rule under sequential loading results in inaccurate estimation of life.

2.2.2. Non-linear damage evolution under a single loading condition

In order to develop a non-linear damage evolution model under sequential loading, an understanding of how damage accumulates under a single loading condition is required. Material damage can be defined as the reduction of resistance to failure. In cyclic loading, fatigue damage increase with applied cycles in a cumulative manner which may lead to fracture. The accumulated damage is related to the applied number of cycles usually through a power-law equation [20].

Wen et al. [21] developed a unified creep and plasticity (UCP) constitutive model for lead-free SnAg solder based on Fine's dislocation energy density and Mura's microcrack initiation theory. A physical damage metric based on percolation theory was developed, which uniquely describes the damage state. The physical damage metric was considered to be a function of the applied number of cycles. A power law relationship between the phenomenological damage parameter and the physical damage metric was proposed as shown in Equation 3 and Figure 9.

Equation 3

$$D = D_c \left(\frac{\omega}{\omega_c} \right)^\eta = D_c \left(\frac{n}{N_f} \right)^\eta$$

where D_c is the critical damage parameter, ω is the microcrack percolation at applied number of cycles, ω_c is the percolation limit, η is the damage exponent, n is the applied number of cycles, and N_f is the cycles to failure.

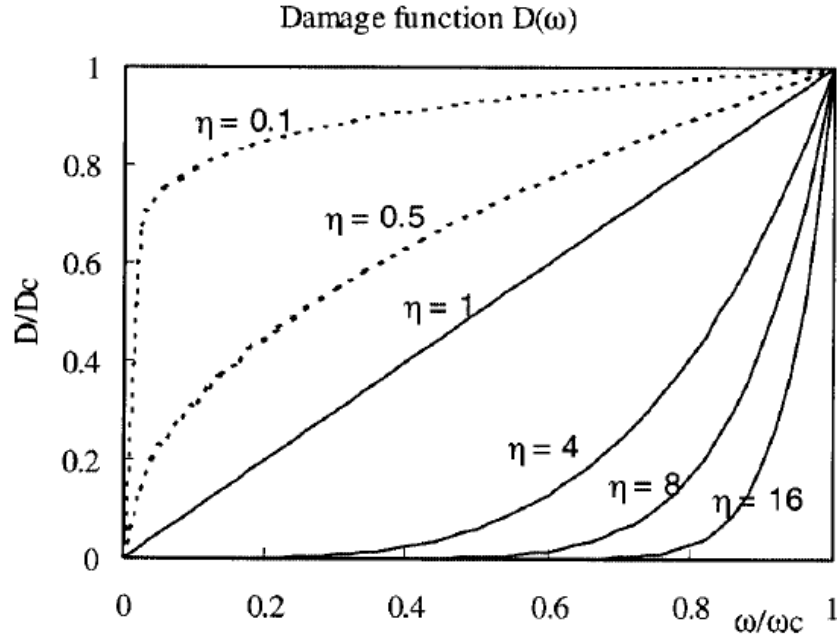


Figure 9. Damage function by Wen et al. [21]

The UCP model was applied on SnAg solder tested under uniaxial strain-controlled isothermal fatigue cyclic loading at 25°C. As a first order approximation, a linear relationship between damage parameter and damage metric was used, i.e., the damage exponent, η , was taken as 1 for Sn3.5Ag solder. Results based on UCP model showed good agreement with the experimental data. Although a non-linear damage accumulation model was proposed for solders under a single load level, the model reduced to Miner's rule formulation for the case of Sn3.5Ag solder studied in [21].

Ladani and Dasgupta [20] proposed an energy partitioning damage evolution model based on the UCP model proposed by Wen et al [21]. The UCP model was based on Mura's theory which is predominantly applicable to plastic deformation caused by dislocation slip and ignores creep mechanisms in lead-free solders due to diffusion-assisted dislocation climb. Hence the UCP was extended by Ladani and

Dasgupta to include the effect of both plastic and creep damage by superpositioning using energy partitioning approach as shown in Equation 4:

Equation 4

$$\frac{D}{D_c} = \left(\frac{n}{N_{fp}} \right)^{\eta_p} + \left(\frac{n}{N_{fc}} \right)^{\eta_c}$$

where D_c is the critical damage parameter, n is the applied number of cycles, η_p is the empirical damage exponent for plastic deformation, N_{fp} is the cycles to failure if only plastic damage occurs, η_c is the empirical damage exponent for creep deformation, and N_{fc} is the cycles to failure if only creep damage occurs.

A notched shear specimen of SAC solder was tested in a thermo-mechanical micro-scale (TMM) test setup to determine the damage exponents for plastic and creep deformations. To isolate plastic deformations, the test was conducted at low temperature of 25°C and high strain rates (5E-2). To isolate creep deformations, another test was conducted at 125°C and low strain rates (5E-4). The damage exponents for plastic and creep deformations at various inelastic strain ranges were obtained experimentally as shown in Figure 10. The damage exponent was assumed to be independent of the load level (cyclic strain range) as no systematic trend was observed. Therefore, the value of damage exponents were averaged over different inelastic strain ranges. For SAC solder, the average values of η_p and η_c was estimated to be 0.47 and 0.52 respectively. However the possibility of a relationship existing between the strain range and damage exponent was not completely rejected in [20].

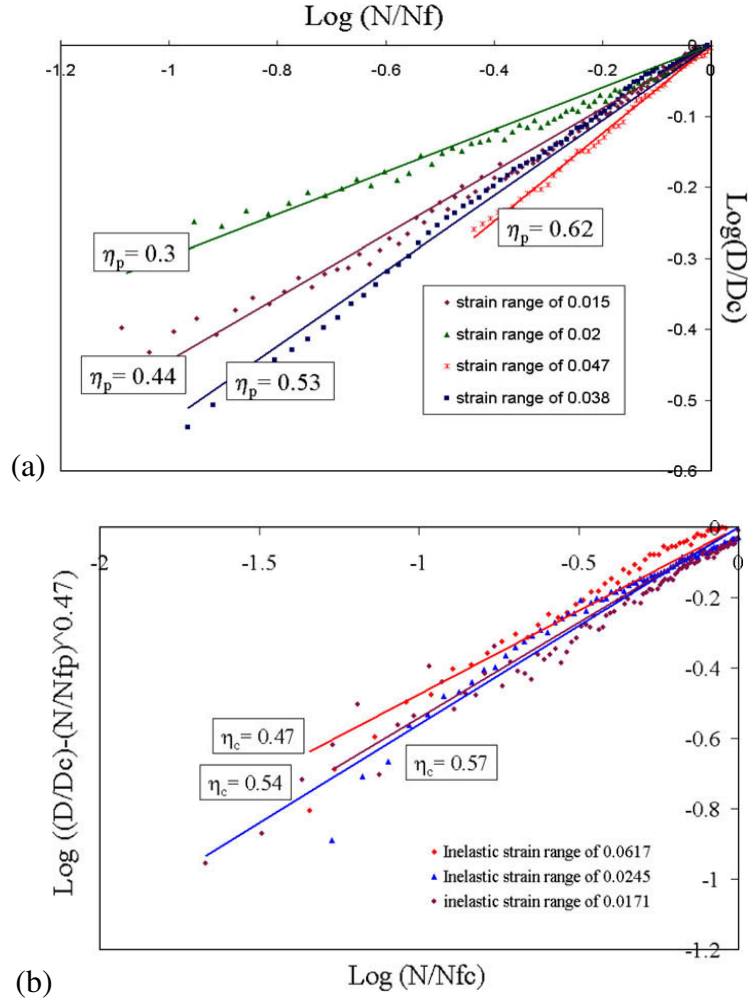


Figure 10. Plot of (a) η_p and (b) η_c for different values of inelastic strain ranges

[20]

Based on the theory of continuum damage mechanics, Xiao et al. [22] proposed a damage evolution model for SAC solder, where the damage is related to the cyclic ratio using a power law. Damage metric was proposed as a function of the electrical resistance of the solder joint as shown in Equation 5.

Equation 5

$$D = 1 - \left(1 - 0.9817 \frac{n}{N_f} \right)^\eta = 1 - \frac{R_0}{R}$$

where n is the applied number of cycles, η is the damage exponent which is 0.154 for SAC solder, N_f is the cycles to failure, R_0 is the original resistance of solder joint and R is the resistance of solder joint.

Thermal cycling test profile (-40°C to 125°C) was carried out on a single joint-shear sample consisting of SAC305 solder alloy and solder resistance was measured every dozens of cycles using four-probe method. The fit of experimental data and proposed damage model results is shown in Figure 11.

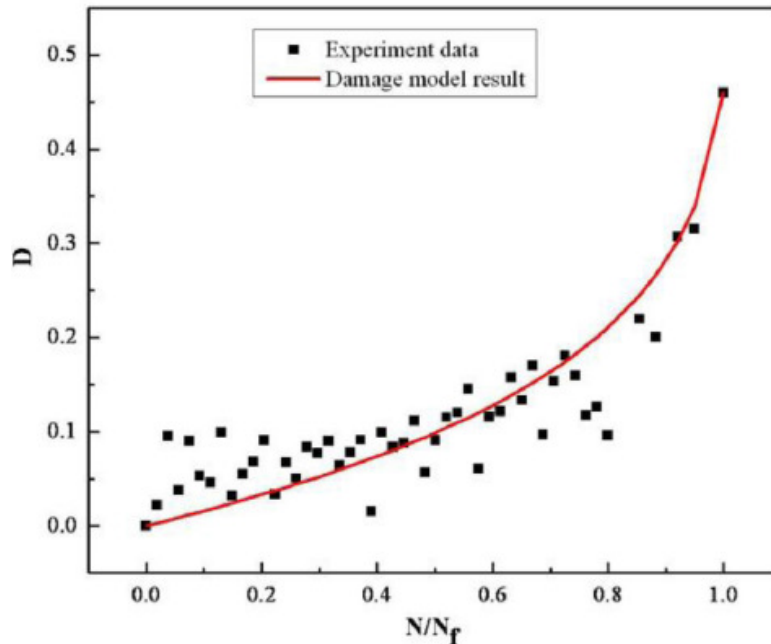


Figure 11. Comparison of experimental and model data [22]

2.2.3. Existing non-linear damage models for solder interconnects under sequential loading

Perkins and Sitaraman [19] developed a non-linear cumulative damage model to study the sequence effect of temperature cycling and vibration loading conditions. The CCGA packages were attached using a high melting point 90Pb10Sn solder

column (2.21 mm high) with a palladium (Pd) doped 63Sn37Pb solder fillet on the substrate side and 63Sn37Pb solder fillet on the board side. These ceramic column grid array (CCGA) packages were subjected to four different types of experimental tests: 1) single step vibration alone to failure (1G input acceleration at natural frequency), 2) single step temperature cycling alone to failure (-25°C to 105°C, 2 cycles per hours), 3) two step loading T-V (temperature cycling for a 50% of N_f from single step temperature cycling followed by vibration to solder joint failure), 4) and two step loading V-T (vibration for $\approx 30\%$ of N_f from single step vibration followed by temperature cycling to solder joint failure).

The results from the two step tests were fitted to a non-linear power law form to obtain the damage exponents under temperature cycling and vibration loading. The η_T and η_V were obtained to be 0.47 and 0.70 for the T-V sequence and 0.91 and 0.93 for the V-T sequence. The authors hypothesized that the numerical value of the damage exponents should be closer to unity for a milder load level. The developed exponents were closer to unity for the vibration load levels and therefore it was concluded that the T-V sequence was harsher than the V-T sequence.

The temperature cycling test conditions were -25°C to 100°C at 2 cycles per minute. For vibration testing, the assemblies were subjected to a 1G input acceleration. Single step temperature cycling and vibration tests were conducted to determine the cycles to failure under single level cyclic loading conditions. The median cycles to failure under single step temperature cycling and vibration tests were 1590 cycles and 1.8E6 cycles respectively (see Table I).

Table I. Cycles to failure for single step test conditions.

	Temperature cycling (cycles)	Vibration (cycles)
	1835	3.10E+06
	1593	2.19E+06
	1587	1.41E+06
	1586	6.07E+05
	1768	
	1474	
Mean	1641	1.83E+06
Median	1590	1.80E+06
Range	361	2.49E+06

For the T-V load sequence, step 1 was temperature cycling and step 2 was vibration testing until solder joint fatigue failure. In the T-V sequence, 800 temperature cycles (50% cycles from standalone test) were applied on 7 samples followed by vibration cycles until failure. Similarly, for the V-T load sequence, step 1 was vibration testing and step 2 was temperature cycling until solder joint fatigue failure. In the V-T sequence, vibration cycles (23-32% cycles from standalone test) were applied on 6 samples followed by temperature cycles until failure. The cumulative damage was determined for the two load sequences using Miner's linear damage rule.

The median value of the cumulative damage using Miner's rule was estimated to be 0.66 for the T-V sequence (see Table II) and 0.96 for the V-T sequence (see Table III). The results from the first two cases of V-T sequences were considered as outliers and were omitted by Perkins (see Table III).

Table II. Cumulative damage using Miner’s rule for T-V load sequence.

T-V load sequence				
Temperature cycling		Vibration		Cumulative damage (Miner)
n_T	n_T/N_T	n_V	n_V/N_V	$n_T/N_T + n_V/N_V$
800	0.5	6.93E+06	0.04	0.54
800	0.5	1.15E+05	0.06	0.57
800	0.5	1.35E+05	0.07	0.58
800	0.5	2.86E+05	0.16	0.66
800	0.5	3.38E+05	0.19	0.69
800	0.5	8.94E+05	0.49	0.99
800	0.5	9.84E+05	0.54	1.04
Mean				0.72
Median				0.66
Range				0.50

Table III. Cumulative damage using Miner’s rule for V-T load sequence.

V-T load sequence				
Vibration		Temperature cycling		Cumulative damage (Miner)
n_V	n_V/N_V	n_T	n_T/N_T	$n_T/N_T + n_V/N_V$
4.35E+05	0.24	23	0.01	0.25 (outlier-not included)
4.15E+05	0.23	24	0.02	0.25 (outlier-not included)
5.76E+05	0.32	890	0.56	0.88
5.33E+05	0.29	1000	0.63	0.92
5.40E+05	0.3	1100	0.69	0.99
4.19E+05	0.23	1300	0.82	1.05
Mean				0.96
Median				0.96
Range				0.17

Since the cumulative damage using Miner's rule was lower than unity for both loading sequences, exponents were fitted to the cycle ratios of each loading condition using regression analysis (Table IV, Table V, Table VI, and Figure 12). However, the regression technique used by Perkins was not reported. It appears that the objective of Perkins was to obtain the lowest error on the median value of the cumulative damage.

Equation 6. T-V sequence

$$D = \left(\frac{n_T}{N_T} \right)^{0.47} + \left(\frac{n_V}{N_V} \right)^{0.70}$$

Table IV. Exponents developed by Perkins for T-V sequence

T-V load sequence		Cumulative damage	
		Miner	Perkins' approach
n_T/N_T	n_V/N_V	$n_T/N_T + n_V/N_V$	$(n_T/N_T)^{0.47} + (n_V/N_V)^{0.70}$
0.5	0.04	0.54	0.83
0.5	0.06	0.57	0.87
0.5	0.07	0.58	0.88
0.5	0.16	0.66	1.00
0.5	0.19	0.69	1.03
0.5	0.49	0.99	1.33
0.5	0.54	1.04	1.37
	Mean	0.72	1.04
	Median	0.66	1.00
	Range	0.50	0.54

Equation 7. V-T sequence

$$D = \left(\frac{n_T}{N_T} \right)^{0.91} + \left(\frac{n_V}{N_V} \right)^{0.93}$$

Table V. Exponents developed by Perkins for V-T sequence.

V-T load sequence		Cumulative damage	
		Miner	Perkins' approach
n_V/N_V	n_T/N_T	$n_T/N_T + n_V/N_V$	$(n_T/N_T)^{0.91} + (n_V/N_V)^{0.93}$
0.32	0.56	0.88	0.93
0.29	0.63	0.92	0.98
0.3	0.69	0.99	1.04
0.23	0.82	1.05	1.09
	Mean	0.96	1.01
	Median	0.96	1.01
	Range	0.17	0.16

Table VI. Exponents determined by Perkins

Perkins' exponents	m_T	m_V
T-V sequence	0.47	0.70
V-T sequence	0.91	0.93

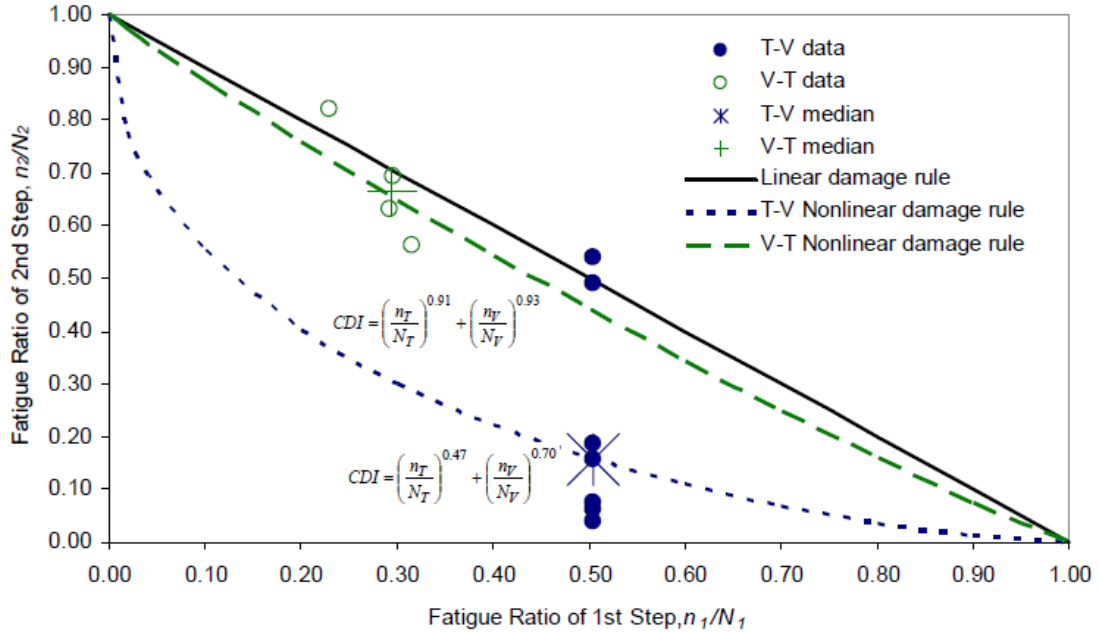


Figure 12. Non-linear fit by Perkins and Sitaraman

Although the median value of the cumulative damage was close to 1 using the regression technique by Perkins, the cumulative damage values for each individual case varied from 0.83 to 1.37, i.e. a range of 0.55 (for the T-V sequence, Table IV) and from 0.93 to 1.09, i.e. a range of 0.16 (for the V-T sequence, Table V).

To verify the exponents developed by Perkins, we carried out a parameter estimation technique based on the maximum likelihood approach. The objective of this parameter estimation was to determine the exponents that provided a cumulative damage close to 1 for each individual case in addition to the median cumulative damage being close to 1. The function used to minimize the error is given in Equation 8:

Equation 8

$$\operatorname{argmin} L(m_T, m_V) = \sum_{i=1}^N \left[1 - \left\{ \left(\frac{n_{t,i}}{N_{f_T}} \right)^{m_T} + \left(\frac{n_{v,i}}{N_{f_V}} \right)^{m_V} \right\} \right]^2$$

The exponents for the T-V sequence determined using the maximum likelihood approach are $m_T = 0.06$ and $m_V = 3$ (see Table VII), and was found to be different from that of Perkins ($m_T = 0.47$ and $m_V = 0.70$). It can be seen from Table VII that the variation on the cumulative damage values (range = 0.157) is lower for the exponents determined from the maximum likelihood approach compared to the exponents determined by Perkins (range = 0.548).

Table VII. Comparison of cumulative damage in T-V sequence using damage exponents developed using the maximum likelihood approach and by Perkins

T-V load sequence		Cumulative damage	
		Perkins' approach	Maximum likelihood approach
n_T/N_T	n_V/N_V	$(n_T/N_T)^{0.47} + (n_V/N_V)^{0.70}$	$(n_T/N_T)^{0.06} + (n_V/N_V)^3$
0.5	0.04	0.83	0.96
0.5	0.06	0.87	0.96
0.5	0.07	0.88	0.96
0.5	0.16	1.00	0.96
0.5	0.19	1.03	0.97
0.5	0.49	1.33	1.08
0.5	0.54	1.37	1.12
	Mean	1.04	1.00
	Median	1.00	0.96
	Range	0.54	0.16

Similarly, the exponents for the V-T sequence (excluding the samples omitted by Perkins) that were determined by the maximum likelihood approach are $m_T = 0.06$

and $m_V = 3$ (see Table VIII). In this case also, the exponents from the maximum likelihood approach were found to be different from that developed by Perkins ($m_T = 0.91$ and $m_V = 0.93$). It can be seen from Table VIII that the variation on the cumulative damage values (range = 0.008) is lower for the exponents determined from the maximum likelihood approach compared to that by Perkins (range = 0.16).

Table VIII. Comparison of cumulative damage in V-T sequence using damage exponents developed using the maximum likelihood approach and by Perkins (first 2 cases omitted by Perkins were omitted in the maximum likelihood approach).

V-T load sequence		Cumulative damage	
		Perkins' approach	Maximum likelihood approach
n_V/N_V	n_T/N_T	$(n_T/N_T)^{0.91} + (n_V/N_V)^{0.93}$	$(n_T/N_T)^{0.06} + (n_V/N_V)^3$
0.32	0.56	0.93	0.999
0.29	0.63	0.98	0.997
0.3	0.69	1.04	1.005
0.23	0.82	1.09	1.000
	Mean	1.01	1.000
	Median	1.01	0.999
	Range	0.16	0.008

Even when the samples (first 2 cases) omitted by Perkins were included in the parameter estimation using the maximum likelihood approach, our approach provided a smaller variation in the cumulative damage values compared to that of Perkins' exponents (see Table IX).

Table IX. Comparison of cumulative damage in V-T sequence using damage exponents developed using the maximum likelihood approach and by Perkins (first 2 cases omitted by Perkins were not omitted in the maximum likelihood approach).

V-T load sequence		Cumulative damage	
		Perkins' approach	Maximum likelihood approach
n_v/N_v	n_T/N_T	$(n_T/N_T)^{0.91} + (n_v/N_v)^{0.93}$	$(n_T/N_T)^{0.06} + (n_v/N_v)^3$
0.24	0.01	0.28	0.77
0.23	0.02	0.27	0.80
0.32	0.56	0.93	1.00
0.29	0.63	0.98	1.00
0.3	0.69	1.04	1.00
0.23	0.82	1.09	1.00
	Mean	0.77	0.93
	Median	0.96	1.00
	Range	0.82	0.23

Analysis of Perkins' data showed that there is no need to use different damage exponents based on the order of the applied load. Perkins exponents varied with the load level because of the regression analysis technique he used to determine the exponents. Additionally, no rationale was provided by Perkins for varying the values of damage exponents when the order of loading was reversed.

The exponents estimated using our approach (maximum likelihood approach) remained the same regardless of the applied load level (see Table X). According to our hypothesis, the exponent is a function of the applied level, i.e. a harsh load will have a low value of damage exponent whereas a mild load has a high value of damage exponent. The temperature cycling test by Perkins is a harsh loading

condition as the mean cycles to failure were approximately 1600 cycles. On the other hand, the vibration test by Perkins is a mild loading condition as the mean cycles to failure was around 1.8E6 cycles. Hence, according to our hypothesis, we expect the damage exponent for the temperature cycling load to be lower than that of the vibration load. The values of exponents ($m_T = 0.06$ and $m_V = 3$) confirm that the hypothesis (that the damage exponents are a function of the applied level) proposed in this dissertation is true.

Table X. Exponents determined from the maximum likelihood approach

Damage exponents	m_T	m_V
T-V sequence	0.06	3
V-T sequence	0.06	3

As discussed in section 2.2.1, since the linear damage rule failed to accurately prediction of damage accumulation under sequential loading, Yang et al. [18] suggested that a non-linear accumulation model in which the damage is proportional to hardness or ductility may work better under sequential loading (see Figure 13). However, an equation to relate the damage to the hardness or ductility and the corresponding parameters were not reported by the authors.

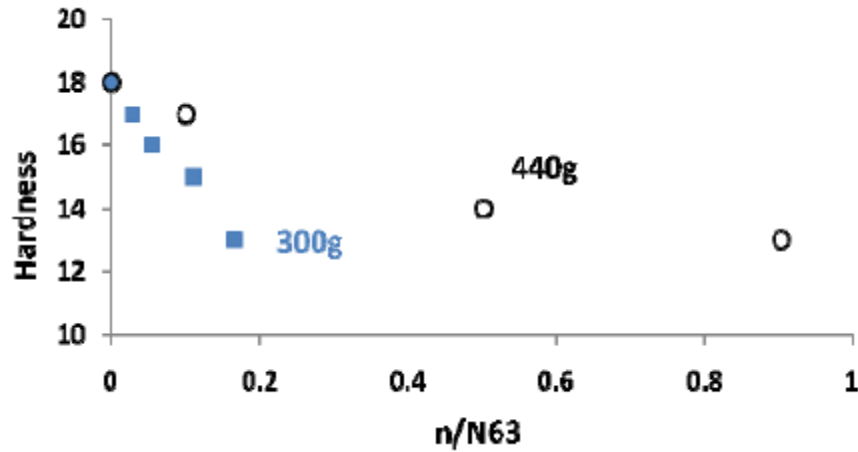


Figure 13. Hardness as a potential damage parameter

Catelani and Scarano [24] proposed a multi-stress accelerated life model able to evaluate the life of tin-silver-copper alloy under combined and sequential tests: cycling climatic and random vibration tests (see Equation 9). The proposed model included two parts: climatic cycling and random vibration. The climatic cycling part of the model was a modified version of the Norris-Landzberg model for thermal cycling test to include relative humidity effects.

Equation 9

$$AF = \frac{N_f}{N_t} = \left(\frac{RH_f}{RH_t} \right)^{-a} \left(\frac{f_f}{f_t} \right)^{-m} \left(\frac{\Delta T_f}{\Delta T_t} \right)^{-n} \left(\exp \left(\frac{E_a}{k} \left(\frac{1}{T_{\max_f}} - \frac{1}{T_{\max_t}} \right) \right) \right)$$

A modified Miner's rule with the exponent as a fitting parameter based on the load type and the sequence of load application was used to estimate the cumulative damage accumulation (see Equation 10).

Equation 10

$$CDI = \left(\frac{n_C}{N_C} \right)^{l_C} + \left(\frac{n_V}{N_V} \right)^{l_V}$$

2.2.4. Existing non-linear damage models for metals under sequential loading

The main deficiencies of Miner's linear damage rule are load-level independence, load-sequence independence and lack of load-interaction accountability. Hence, soon after the development of Miner's rule in 1945, various researchers have looked into non-linear damage accumulation methods to account for the load-sequence effect. One of the earliest non-linear damage accumulation models was proposed by Marco and Starkey.

Marco and Starkey Model

To address the deficiencies of Miner's rule, Richart and Newmark [25] in 1948 proposed the concept of damage curves and speculated that damage vs. cycle ratio curves are different at different load levels. In 1954, Marco and Starkey [26] proposed the first nonlinear load-dependent damage theory represented by a power relationship (see Equation 11):

Equation 11

$$D = \sum r_i^{x_i}$$

where x_i is a variable quantity related to the i^{th} loading level. The model was developed based on the concept proposed by Richart and Newmark and results from load sequence experiments. According to Marco and Starkey, the damage exponent at a specific load level is a variable quantity related to that loading level and the damage

paths varied based on the level of the applied load (see Figure 14). The non-linear model took into account the effect of reversal of load sequences. Although Marco and Starkey proposed a non-linear model, the relation between the damage exponent and the applied load level/life was not defined. Hence, experiments were required to be conducted every time a new loading condition is encountered.

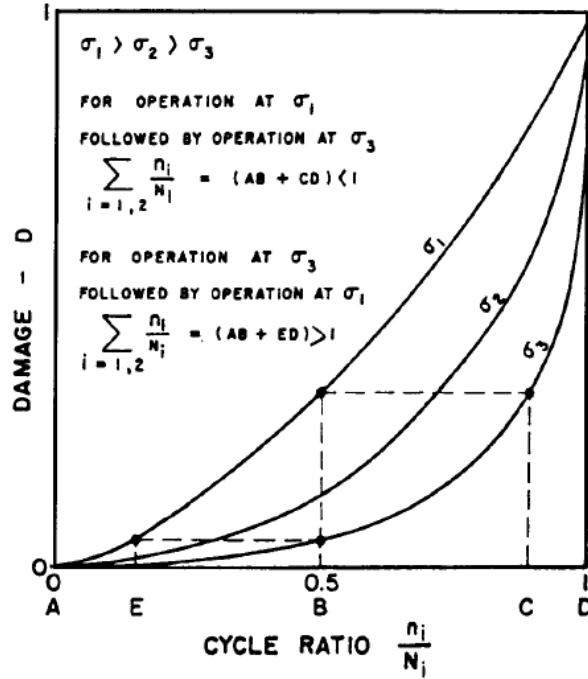


Figure 14. Marco and Starkey approach

Damage Curve Approach by Manson and Halford

Manson and Halford [27] developed a generalized relationship between the damage exponent and the cycles to failure based on crack initiation and propagation in steel and aluminum specimens. A model for damage accumulation was established based on an effective crack growth equation. A relationship (Equation 12) for the number of cycles required to develop a crack 0.003 inches deep in terms of cycles to failure of a 1/4 inch test specimen was given as:

Equation 12

$$N_{0.003} = N_f - 2.5N_f^{2/3}$$

Similarly the relationship (Equation 13) for the number of cycles required to develop a crack 0.013 inches deep in terms of cycles to failure was given as:

Equation 13

$$N_{0.013} = N_f - 4N_f^{0.6}$$

Manson and Halford claimed that both the equations were empirical and their forms were chosen to fit experimental results. For further analysis the authors pursued the following generalized form for crack propagation under cyclic loading (see Equation 14).

Equation 14

$$a = a_0 + (0.18 - a_0)(n_a / N_f)^{(2/3)N_f^{0.4}}$$

where a is the crack length at n_a number of applied cycles, a_0 is the initial crack length, and N_f is the cycles to failure under that load level.

Manson considered damage to be analogous to crack growth and assumed that crack growth was related to applied number of cycles using a power law with the exponent as a function of cycles to failure. The crack propagation relation provided in Equation 14 was normalized to obtain a relationship for damage versus applied number of cycles as shown in Equation 15.

reasoning. Additionally, the applicability of Manson's non-linear form has not been validated for solder material.

2.3. Mapping of damage under different loading conditions

In this section, studies in the literature addressing the transformation of the damage accumulated under one stress level/load condition relative to another stress level/load condition are reviewed. Under the same loading type, acceleration factors (AF) are most widely used to transform the damage relative to different load levels. With respect to life, AF is defined as the linear ratio of the cycles to failure under stress level 1 to that under stress level 2. Since there is an inherent assumption of linear damage accumulation, for the same stress levels the AF is defined as the ratio of damage under stress level 1 to that under stress level 2 as shown in Equation 17.

Equation 17

$$AF = \frac{N_1}{N_2} = \frac{D_2}{D_1}$$

In a study by Lall et al. [23], the concept of damage mapping or damage equivalency relationships between isothermal aging and thermal cycling was provided as shown in Figure 16. PBGA packages (456 I/O) soldered using eutectic tin-lead alloy were subjected to isothermal aging at 60°C and phase growth was quantified at varying lengths of time to determine the damage metric as shown by Equation 18.

Equation 18

$$D_{iso} = \left(\frac{g_n}{g_0} \right)^4 - 1 = a_{iso} (t)^{b_{iso}}$$

where D_{iso} is the damage metric under isothermal aging condition, g_t is the phase growth at time t , g_0 is the initial phase size, a_{iso} and b_{iso} are the fitted model constants, and t is the aging time in hours. Similarly, temperature cycling was carried out on another set of samples between -40°C and 125°C at 2.5 hours per cycle. Phase growth was quantified at specified intervals of cycles to determine the damage metric as shown in Equation 19.

Equation 19

$$D_{TC} = \left(\frac{g_N}{g_0} \right)^4 - 1 = a_{TC} (N)^{b_{TC}}$$

where D_{TC} is the damage metric under temperature cycling condition, g_N is the phase growth at N^{th} cycle, g_0 is the initial phase size, a_{TC} and b_{TC} are the fitted model constants, and N is the number of cycles. Damage equivalence was achieved by equating (7) and (8) as shown in Equation 20 and Figure 16.

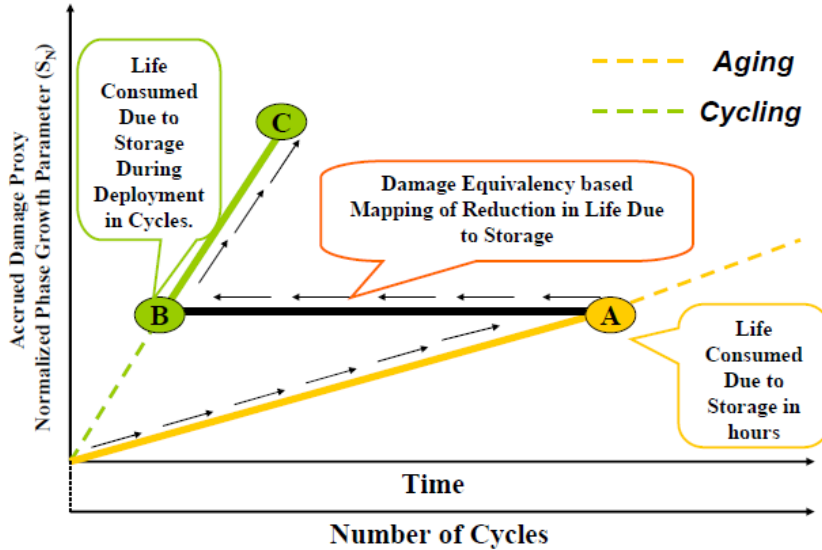


Figure 16. Schematic of damage mapping between isothermal aging and temperature cycling [23]

Equation 20

$$D = a_{TC} (N)^{b_{TC}} = a_{iso} (t)^{b_{iso}}$$

Similarly, damage metric based on IMC thickness growth during isothermal aging and temperature cycling conditions was developed. The damage equivalence between thermal aging and thermal cycling from experimental data is shown in Figure 17. No experimental testing was carried out using sequential loading conditions to verify the applicability under sequential loading.

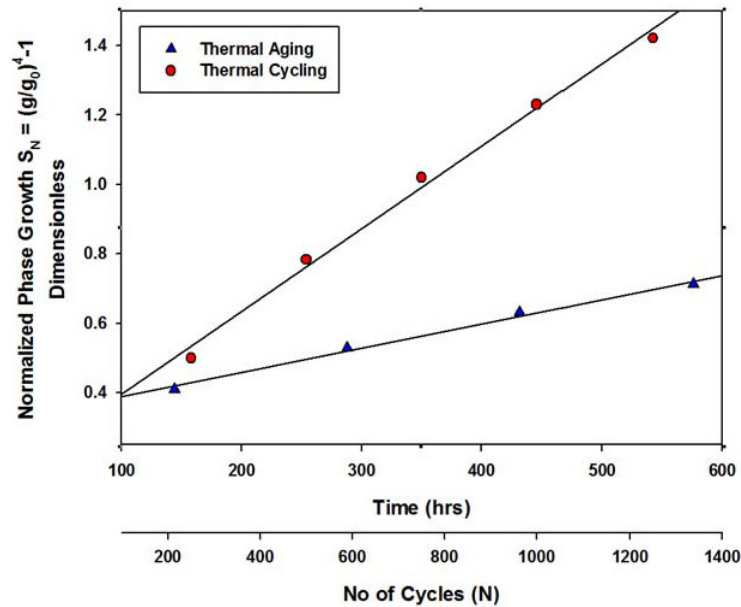


Figure 17. Damage mapping between isothermal aging and temperature cycling using phase growth model [23]

2.4. Gaps in existing research

Despite the inherent limitations and inaccuracies, Miner's rule is widely used in damage estimation. Although various studies in the literature have illustrated these inaccuracies, very few studies have provided alternatives to Miner's rule for solder interconnects. While Miner's rule estimations may be sufficient for a single cyclic

condition or conditions with only slight variations, the results from the literature point to a systemic issue with the linear damage accumulation approach. Further, the literature points to a load independence of damage accumulation. Therefore, there is a need for a non-linear damage model to accurately predict the damage under sequential loading conditions. However, very limited studies have focused on the non-linear accumulation of damage in solder interconnects under sequential loading.

The damage evolution models under a single loading condition developed by Wen et al. [21], Ladani and Dasgupta [20], and Xiao et al. [22] showed that damage and cycle ratio follow a power law relationship. However, the damage exponents have been assumed to be a constant and the dependence of the exponent on the applied load level (cycles to failure) has not been evaluated. The applicability of the above models under sequential loading conditions was also not evaluated. The non-linear damage accumulation model for sequential proposed by Perkins and Sitaraman [19] requires extensive experimental testing and the value of damage exponents developed varied when the sequence of loading conditions is switched. Our analysis showed that there was not rationale for changing the value of damage exponent for a particular load type/level when the order of load application was switched. In addition, the dependence of damage exponents on the stress levels was not evaluated. The plot of damage exponent versus strain range from the study by Ladani and Dasgupta [20] revealed that the damage exponent varied with change in strain range, as shown in Figure 18. From the literature review, it can be concluded that a cumulative damage assessment model considering the sequence and type of loading conditions is not available for solder interconnects.

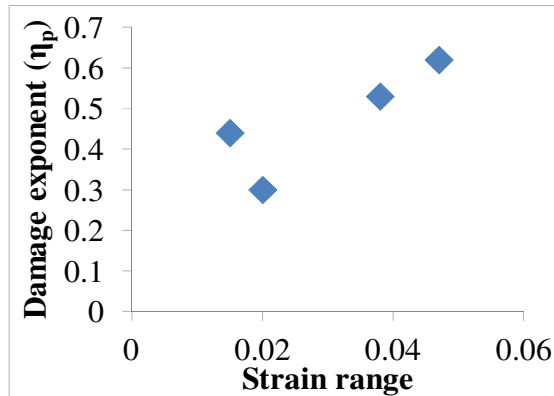


Figure 18. Dependence of damage exponent on strain range (adapted from [20])

Lall et al. [23] proposed the concept of damage mapping between isothermal aging and temperature cycling for solder interconnects. However, it has been shown in the literature that the damage under isothermal preconditioning need not necessarily increase monotonically and can result in improved cycles to failure under temperature cycling. Experimental validation by sequential loading was also not carried out. Hence, a methodology to compare and map the damage under different load levels is not available.

2.5. Dissertation objectives

The primary objective of this dissertation is to develop an approach to experimentally determine load dependent damage exponents for solder interconnects under sequential cyclic loading conditions. These load dependent damage exponents are required to create a non-linear damage accumulation model for solder interconnects. The proposed non-linear model should consider the effects of load levels and sequence of applied loading conditions.

For the purpose of this dissertation, a sequential loading is defined as the application of a cyclic loading condition followed by another cyclic loading condition

of a different load level. The cyclic loading condition referred to in this dissertation is limited to cyclic shear loads at different load levels.

Another objective of this dissertation is to develop an analytical relationship between the damage exponent function and the applied load level. This will enable the development of a model that does not require experiments to be carried out when new loading conditions are encountered.

Chapter 3: Development of a Load Dependent Non-linear Damage Model for Sequential Loading

A load dependent non-linear model which takes into account the effect of sequence of loads under sequential loading of solder interconnects is proposed in this chapter.

3.1. Load dependent non-linear damage model

The non-linear damage forms proposed for steel and aluminum specimens generally followed a power law relationship. In this form damage is related to the ratio of the applied number of cycles to cycles to failure in a power relationship where the power exponent is a function of the applied load level, as shown in Equation 21:

Equation 21

$$D = \sum (r_i)^{F(N_{fi})} = \sum \left(\frac{n_i}{N_{fi}} \right)^{F(N_{fi})}$$

where n_i is the applied cycles in i^{th} stress level, N_i is the cycles to failure in i^{th} stress level, and $F(N_{fi})$ is the damage exponent at i^{th} stress level. The damage exponent is defined as a function of the applied load level, which may be represented by the Nf for the applied load level. According to the non-linear damage model, the damage accumulation proceeds along the curve associated with the load level at which a cycle ratio is applied as shown in Figure 19. This results in non-coincident curves for each load level. For instance, when the solders are subjected to the same cycle ratio at two different load levels, the damage states are not equivalent.

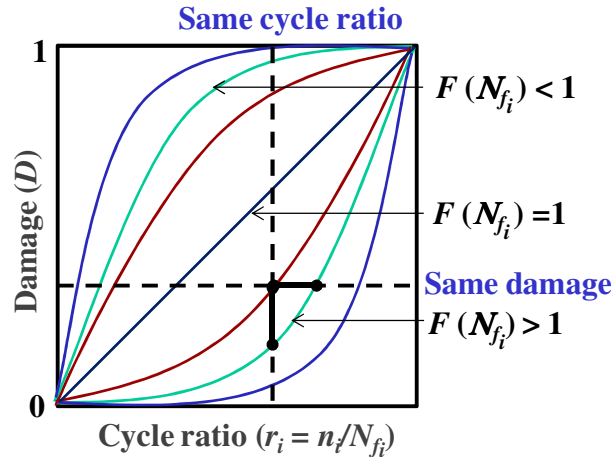


Figure 19. Damage curve at different life/load levels

Miner's rule requires that the damage curves to be coincident at all load levels. It is the separateness of damage curves at different load levels in a non-linear model that accommodates the loading order or sequence effect. All curves initiate at the origin where the damage is considered to be zero ($D=0$) and terminate at failure where the damage is unity ($D=1$).

The incorporation of the sequence effect by a non-linear damage model is illustrated by considering a harsh-mild load sequence and a mild-harsh load sequence. During a harsh-mild load sequence, when n_1 cycles of a harsh load (life level N_{f1}) is first applied, the damage will proceed from zero to A along the path as shown in Figure 20. At this juncture, when a milder load level (life level N_{f2}) is introduced, the equivalent cycles of the mild load that cause the same amount of damage as n_1 harsh cycles is given as n_2 . This is under the assumption that damage at B is at the same damage as A i.e., no additional damage was introduced when between the application of the loading conditions. Now, if the mild load is applied until failure, $n_{2\text{-remaining}}$ is the remaining cycles, such that failure occurs at C. In the harsh-mild load sequence,

when the first loading is applied the damage accumulates along 0A and for the second loading along BC. If the sum of cycle ratios were considered according to Miner's rule, the cycle ratio in the distance AB will be omitted resulting in an inaccurate estimate.

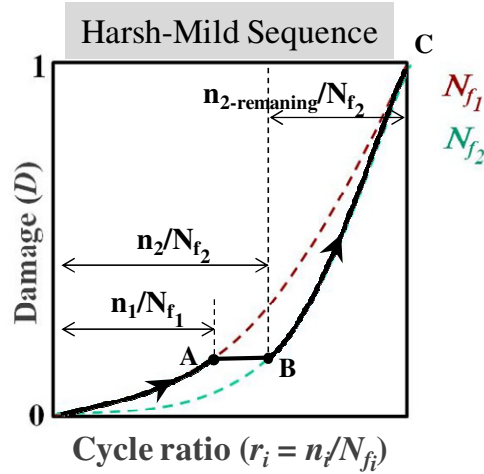


Figure 20. Effect of load sequence in a non-linear damage model under a harsh-mild load sequence

Equation 22

$$n_2 = N_{f_2} \left(\frac{n_1}{N_{f_1}} \right)^{F(N_{f_1})/F(N_{f_2})}$$

Remaining cycles to failure under mild loading condition:

$$= N_{f_2} - n_2 = N_{f_2} \left[1 - \left(\frac{n_1}{N_{f_1}} \right)^{F(N_{f_1})/F(N_{f_2})} \right]$$

On the other hand, in a mild-harsh load sequence, the damage accumulation path is along 0B when n_2 mild cycles are applied (see Figure 21). When a harsh load is introduced, the harsh cycles equivalent to n_2 mild cycles is given as n_1 . Therefore, in a

mild-harsh load sequence, the first loading results in damage accumulation along 0B and the second loading along AC. In this case, the summation of cycle ratio according to Miner's rule includes the distance AB twice resulting in an inaccurate estimate.

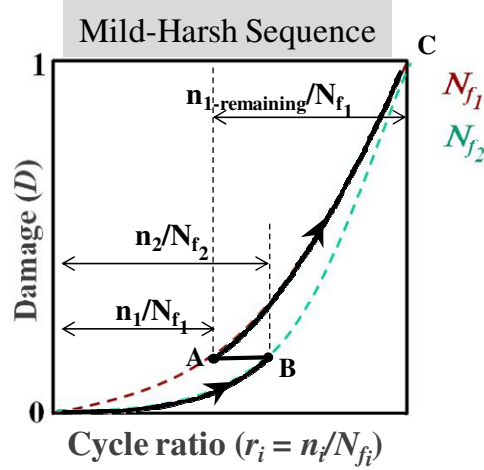


Figure 21. Effect of load sequence in a non-linear damage model under mild-harsh load sequence

Equation 23

$$n_1 = N_{f_1} \left(\frac{n_2}{N_{f_2}} \right)^{\frac{F(N_{f_2})}{F(N_{f_1})}}$$

Remaining cycles to failure under harsh loading condition:

$$= N_{f_1} - n_1 = N_{f_1} \left[1 - \left(\frac{n_2}{N_{f_2}} \right)^{\frac{F(N_{f_2})}{F(N_{f_1})}} \right]$$

To illustrate the capability of the damage curve approach to take into account the load sequence effect, a simulation exercise was carried out. According to our hypothesis, the damage exponent increases as the level of harshness is decreased for the load level. Therefore a mild loading condition will have a higher numerical value

of damage exponent than harsh loading condition. Let us assume the damage exponent to be 2 for the harsh loading condition and 4 for the mild loading condition. The cycles to failure (N_f) for the harsh and mild loading conditions are assumed to be 5000 and 10000 cycles respectively. After application of 2500 cycles of the harsh loading condition, according to Miner's rule the solder would be at 0.5 damage. If a non-linear damage curve approach is used, then the corresponding damage is 0.25 at the end of application of harsh loading. According to Miner's rule the remaining damage in the mild loading condition is 0.5 whereas according to damage curve approach, remaining damage is 0.75. Damage accumulation using Miner's rule and damage curve approach during a harsh-mild loading condition are shown in Figure 22 and Figure 23.

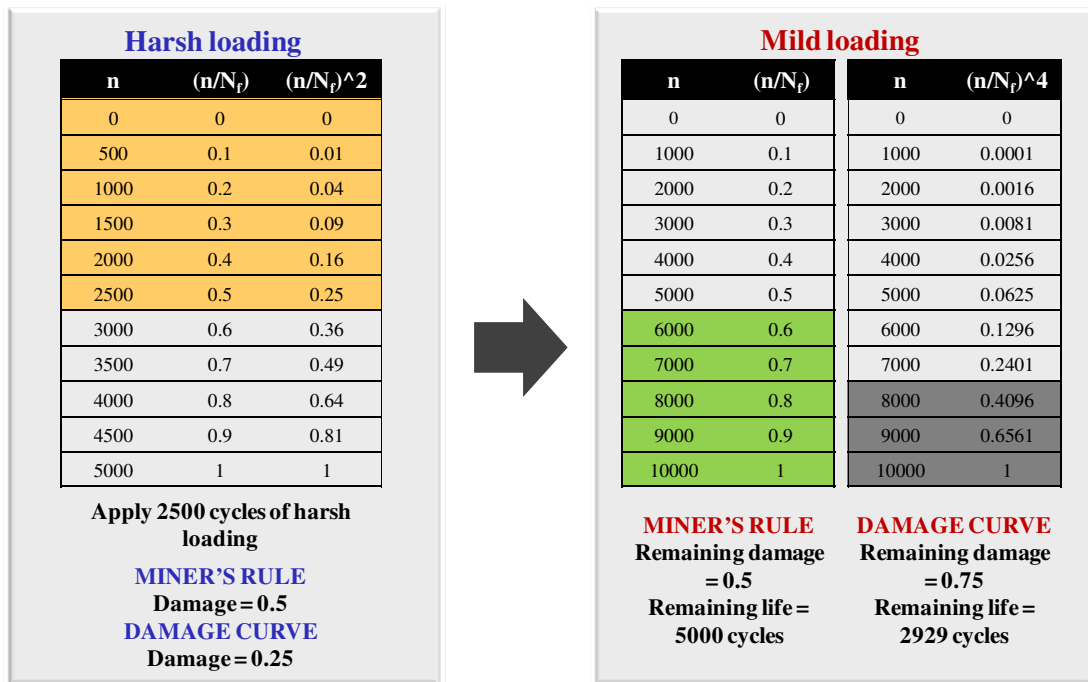


Figure 22. Simulation of cycle counts under a harsh-mild loading condition

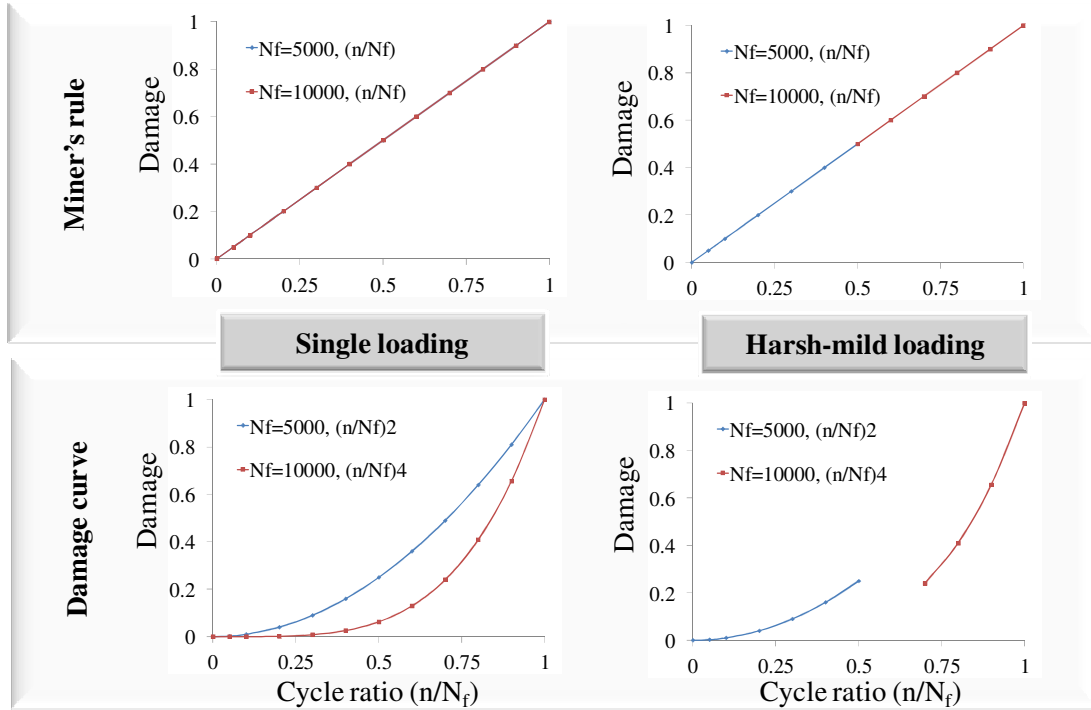


Figure 23. Simulation of damage propagation under a harsh-mild loading condition

3.2. Experimental approach to create damage curves

The experimental approach to create damage curves is broadly classified into three sets (see Figure 24). The first set of tests was conducted to determine the cycles to failure for each load level (N_f). As explained earlier, tests were conducted at three different load levels. In the second set of tests, sequential tests were carried out, where a fixed number of cycles of the first load level is applied followed by the next load level until failure. Using the combination of the single step and sequential tests, damage curves for solder interconnects can be experimentally determined for the three load levels. The third set of tests includes tests to experimentally validate the developed damage curves. These tests include the reversal of load of sequence and application of a new loading condition.

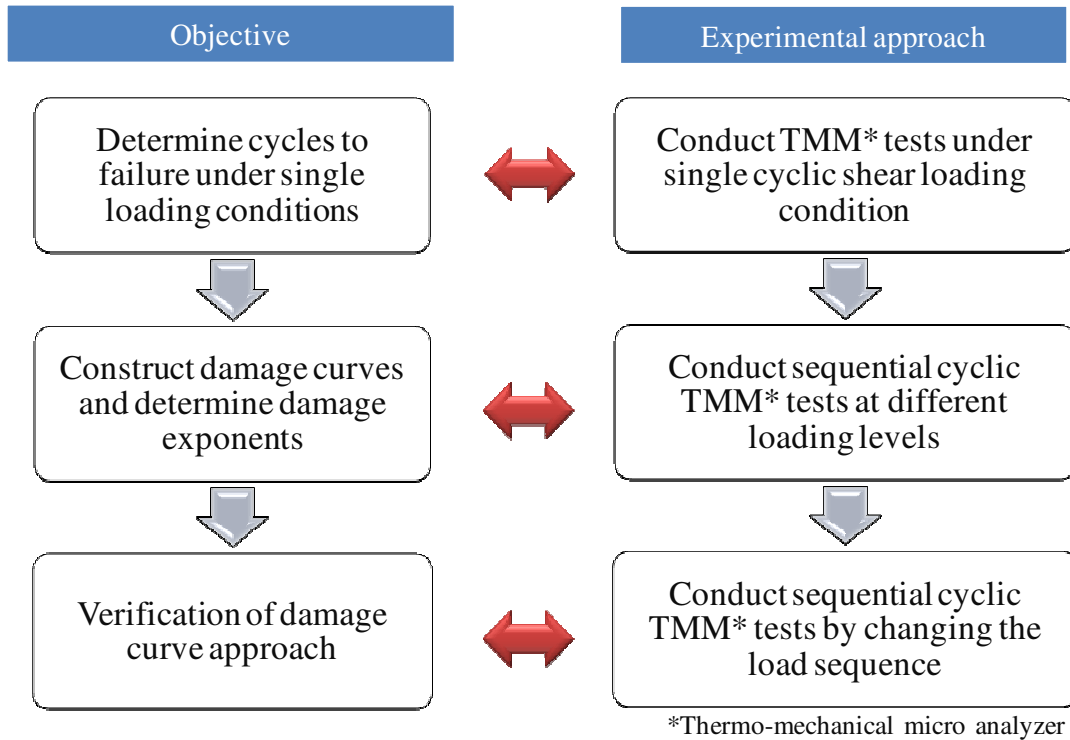


Figure 24. Experimental approach to develop damage curves

3.2.1. Determination of damage exponents

The procedure to experimentally determine the damage exponents at two different load levels by conducting sequential tests is explained (see Figure 25). Two sets of sequential tests are required to determine the damage exponents at two load levels. In the first set of sequential tests, n_{0A} cycles of the first load level (N_{f1}) are applied followed by the second load level (N_{f2}) until failure. Since the damage levels at A and B are same, the cycle ratios of the two load levels are related as shown in Equation 24. Considering that damage value is unity at the time of failure, the damage equation under sequential loading (see Equation 25). In Equation 25, the damage exponents for the two load levels ($F(N_{f1})$ and $F(N_{f2})$) are unknown whereas the values of n_{0A} , N_{f1} , n_{BC} , and N_{f2} are obtained from sequential tests.

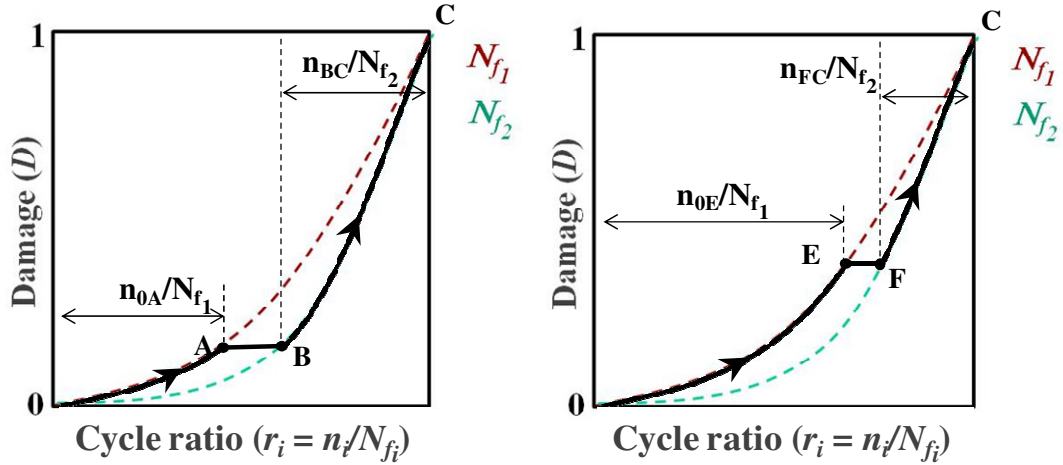


Figure 25. Determination of damage exponents from two sets of sequential tests

Equation 24

$$D_1(n_{0A}) = D_2(n_{0B}) \quad i.e. \quad \left(\frac{n_{0A}}{N_{f1}} \right)^{F(N_{f1})} = \left(\frac{n_{0B}}{N_{f2}} \right)^{F(N_{f2})}$$

Equation 25

$$1 = \left(\frac{n_{0B}}{N_{f2}} \right)^{F(N_{f2})} + \left(\frac{n_{BC}}{N_{f2}} \right)^{F(N_{f2})} = \left(\frac{n_{0A}}{N_{f1}} \right)^{F(N_{f1})} + \left(\frac{n_{BC}}{N_{f2}} \right)^{F(N_{f2})}$$

Similarly, in the second set of sequential tests, a different number of cycles (n_{0E}) of the first load level (N_{f1}) are applied followed by the second load level (N_{f2}) until failure. The damage equation under sequential loading for this set is given in Equation 26. Similar to Equation 26, the damage exponents for the two load levels ($F(N_{f1})$ and $F(N_{f2})$) in Equation 25 are unknown whereas the values of n_{0E} , N_{f1} , n_{FC} , and N_{f2} are obtained from sequential tests. Therefore, from two sets of sequential tests, the two unknowns ($F(N_{f1})$ and $F(N_{f2})$) can be solved from the two equations (Equation 25 and Equation 26).

Equation 26

$$1 = \left(\frac{n_{0F}}{N_{f2}} \right)^{F(N_{f2})} + \left(\frac{n_{FC}}{N_{f2}} \right)^{F(N_{f2})} = \left(\frac{n_{0E}}{N_{f1}} \right)^{F(N_{f1})} + \left(\frac{n_{FC}}{N_{f2}} \right)^{F(N_{f2})}$$

where the damage exponents are functions of cycles to failure under single loading condition, $F(N_{f1})$ and $F(N_{f2})$

Two sets of single level cyclic tests and two sets of ‘sequential’ tests are required for the experimental determination of damage exponents at two load levels. If an analytical relation between the load level and damage exponent is developed, then experiments are not required to be carried out for each new load level. The damage exponent for a third load level is determined using the procedure explained earlier. From three damage exponents and their corresponding load levels, an analytical relationship between the damage exponent and applied load level can be developed.

The three load levels were defined as load level 1, load level 2, and load level 3 based on the applied displacement/ISR (see Figure 26). The applied displacement/ISR decreased from load level 1 through 3. Tests 1 through 3 were conducted to determine the cycles to failure (N_f) under standalone loading conditions. The cycles to failure data from tests 1, 2, 4 and 5 were substituted in Equation 25 to determine the damage exponents for load levels 1 and 2. Similarly, the cycles to failure data from tests 1, 3, and 6 along with the harsh load level exponent were substituted in Equation 26 to obtain the damage exponent for the load level 3. A detailed description of the experimentation is provided in Chapter 4.

	Test No.	Load level 1 ISR = 0.215	Load level 2 ISR = 0.107	Load level 3 ISR = 0.039	Sample size
Development	1	until failure			3
	2	until failure			3
	3	until failure			3
	4	30% load drop	→	until failure	3
	5	60% load drop	→	until failure	3
	6	30% load drop	→ until failure		3
Validation	7	60% load drop	→ until failure		2
	8	until failure	←	30% load drop	1
	9	until failure	←	30% load drop	1
	10	until failure	← 30% load drop		1

Figure 26. Experimental suite to determine damage curves at three load levels.

3.2.2. Damage exponent vs load level relationship

Development of an analytical relationship between damage exponent and cycles to failure (N_f) can assist in creating damage curves at various load levels without conducting experiments for each test condition. The damage exponent can then be defined as a function of strain range or inelastic strain energy using existing solder joint fatigue models. As the load level increases, damage accumulates at a faster rate. From a physical standpoint, there will be considerable damage accumulation during the initial period of cycling at a higher load level compared to a lower load level. As the load level is increased, the value of damage exponent (η) will tend to be closer to 1 as shown in Figure 27.

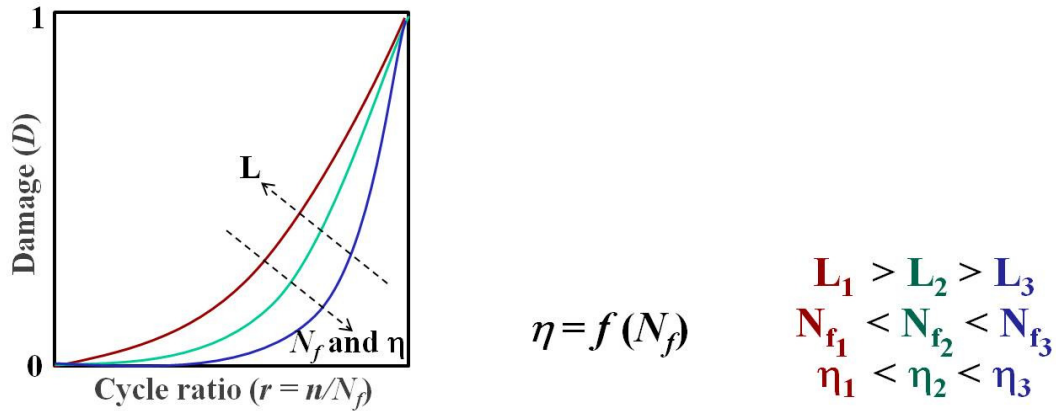


Figure 27. Dependence of damage exponents on load levels and life

The damage exponent will be a function of the cycles to failure (N_f) which in turn is a function of inelastic strain range or strain energy. Using existing life prediction analytical models like Engelmaier model, the cycles to failure in a temperature cycling condition can be related to the inelastic strain range which is a function of the applied temperature range, mean temperature, dwell time, package geometry, solder geometry and material. Thus the damage exponents can be related to various cycling profile and material parameters. Similarly analytical models like modified Basquin's model can be used in the case of mechanical bend cycling. The use of energy based models in conjunction with finite element analysis can be used to relate the life to inelastic strain energy or total strain energy.

3.2.3. Damage mapping between load levels and load types

The non-linear nature of damage curves results in non-coincident damage curves for different load levels and conditions. The construction of damage curves in section 0 will enable mapping of the damage accumulated under different load levels and load types as shown in Figure 28 and Figure 29. The remaining cycles to failure under

different load levels and conditions can therefore be estimated. For instance, when solder interconnects are subjected to 50% of damage under temperature cycling, the equivalent damage accumulated under mechanical bend cycling can be determined using the damage curves. Damage mapping is also useful in estimating the remaining useful life of an already damaged solder interconnect under different load levels and load types. For instance, when solder interconnects are subjected to 50% of damage under a particular temperature cycling profile, it can undergo 50% of damage under the same temperature cycling profile or X% of damage under another temperature cycling or mechanical bend profile estimated using damage curves. The damage mapping or equivalency relationship for two different load level/type is shown in Equation 27.

Equation 27

$$n_2 = N_{f_2} \left(\frac{n_1}{N_{f_1}} \right)^{F(N_{f_1})/F(N_{f_2})}$$

where the damage exponents are functions of cycles to failure under single loading condition, $\eta_1 = f(N_{f1})$ and $\eta_2 = f(N_{f2})$

The non-linear nature of damage curves results in non-coincident damage curves for different load levels and conditions. Hence, in addition to damage mapping, the remaining cycles to failure under a new load level can therefore be estimated for solder interconnects. The developed damage exponent function $F(N_f)$ will be dependent on the solder material and the cycles to failure under that loading condition.

Remaining cycles to failure under second loading condition:

$$= N_{f_2} - n_2 = N_{f_2} \left[1 - \left(\frac{n_1}{N_{f_1}} \right)^{F(N_{f_1})/F(N_{f_2})} \right]$$

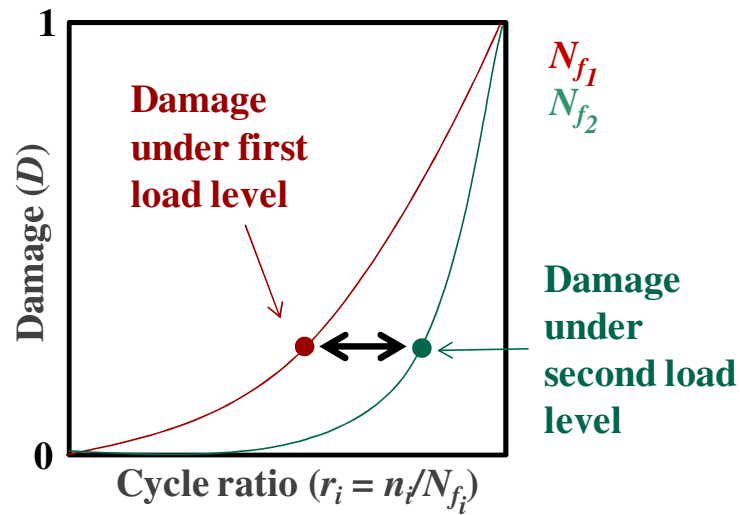


Figure 28. Damage mapping for different load levels

An additional factor may be required to map damage between temperature cycling and cyclic mechanical bend. Since creep occurs in temperature cycling tests in addition to fatigue loading compared to cyclic mechanical bend, the microstructures may be at a different state. Damage mapping for different load types is not studied in this dissertation. However, the experimental methodology developed in this study may be extended with further experimentation to include damage mapping under different load types as well.

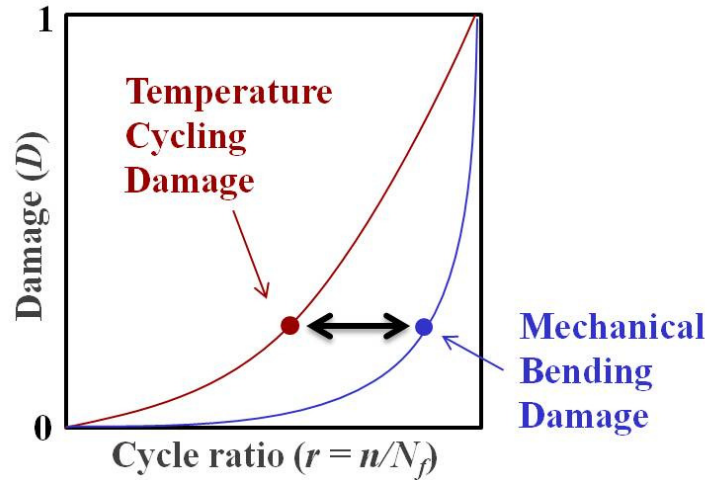


Figure 29. Damage mapping for different load types

3.2.3. Assumptions/limitations of the approach

In single step tests, since more than one sample is tested a distribution of cycles to failure is obtained as opposed to a single value of N_f . Hence, a distribution has to be assumed representing the failure mechanism and a distribution parameter ($N_{1\%}$, $N_{50\%}$ or characteristic life) should be used to represent the values of cycles to failure (see Figure 30). The distribution parameter should be selected such that no samples have started failing during the application of a predefined number of cycles under the first load level. The same distribution parameter will be utilized to represent remaining cycles to failure under the second load level. The selection of distribution parameter will depend on the application condition in which the solder interconnects will be employed. For instance, in critical applications $N_{1\%}$ may be the parameter of interest since the customer/application requirements are stringent such that no failures are acceptable. For this study, the value of $N_{50\%}$ will be used for the construction of damage curves.

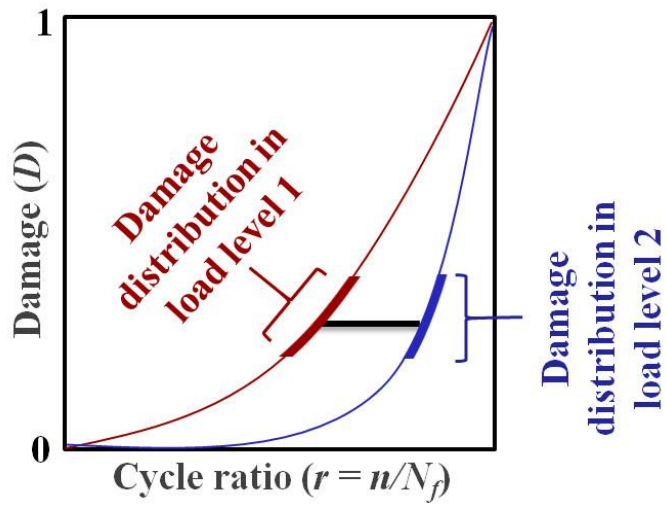


Figure 30. Damage distributions

Chapter 4: Experimental Setup

The thermo-mechanical micro (TMM) analyzer test apparatus used in the experimental approach has been described in the literature [28]. TMM is a custom-built mechanical testing system for conducting isothermal monotonic constitutive tests as well as cyclic mechanical fatigue tests. The system is depicted in Figure 31.

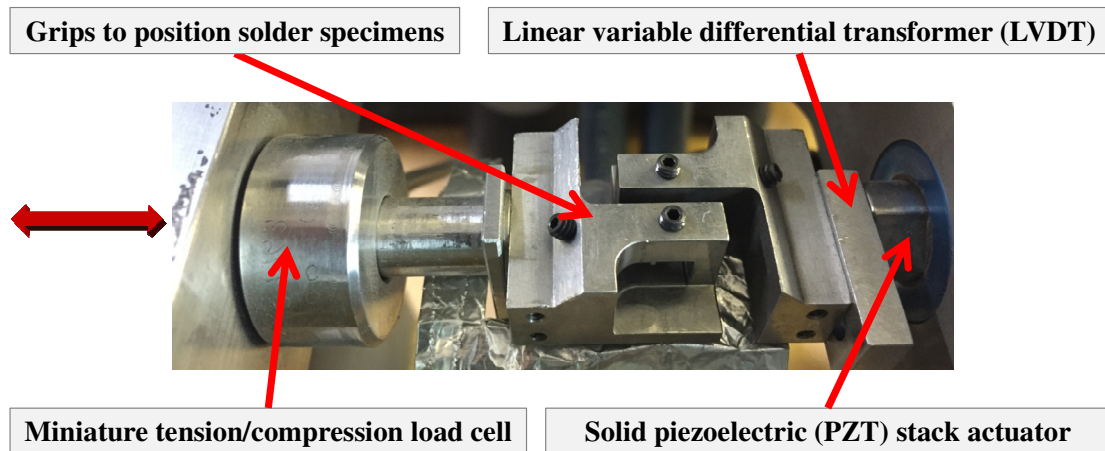


Figure 31 (a) TMM test setup

The cyclic displacements are produced by a stack actuator. Solid piezoelectric (PZT) stack actuator applies controlled amounts of displacement to the specimen grips over a range of $90\mu\text{m}$ in a closed loop displacement controlled system through a flexible link, a low friction linear bushing and a connecting shaft. Displacements in the solder are obtained by adjusting for load train stiffness. The applied deformation is measured and controlled using a Solartron linear variable differential transformer (LVDT) spanning the specimen grips. The force is measured using a 445 N (100 lb.) capacity miniature tension/compression load cell (Sensotec Model 31) with a resolution of approximately 0.1 N. A Keithley-Metrabyte DAS1802HR-DA data

acquisition card with a 16-bit digital-to-analog and analog-to-digital converter is used to collect test data as well as provide a control signal to the PZT actuator.

Thermo-mechanical micro-scale (TMM) analyzer enables experimental testing of solder alloy specimens with length scales similar to those seen in typical solder interconnects. TMM has four available control schemes to conduct cyclic tests: total displacement, total deformation, inelastic deformation, and work dissipation. For the purpose of this dissertation, inelastic strain range (ISR) controlled testing was carried out in the TMM test setup since time independent inelastic (plastic) strain is the primary cause of solder joint fatigue failure. This enables to define the load level as a function of the ISR and therefore can be provided as the input to the non-linear damage model (see Figure 32). Since ISR can be estimated using finite element analysis or analytical models, there is no need to repeat tests for new load levels. Also, commonly used strain range based models like Coffin-Manson can be used to estimate ISR values which can in turn be provided as an input to the proposed non-linear damage accumulation model. The TMM test frame has been characterized thereby enabling the estimation of strain in the solder joint.

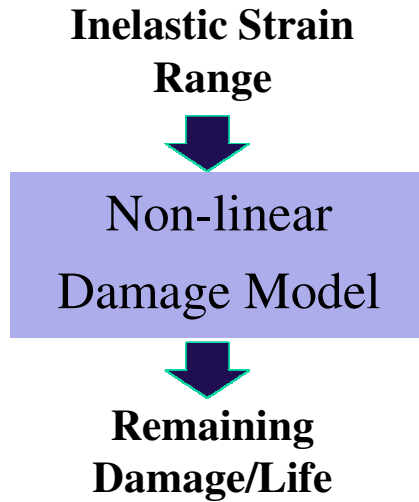


Figure 32. Input and output of the proposed non-linear damage model

4.1 Test specimen

A modified notched shear specimen proposed by Iosipescu was used to conduct shear tests in TMM (see Figure 33 and Figure 34). The solder experiences a reasonably uniform stress distribution due to the 90° notch angles (see Figure 35). Copper was used as the platen material to mimic the pad in an actual microelectronic device. The copper platens do not have any metallization layers and the solder behavior corresponds to those on printed wiring boards with Organic Solder Preservative (OSP) and immersion Sn pad finish. The solder joint widths were in the range of 180-200 μm . Soldering was carried out at 30°C higher than the liquidus temperature (T_{melt}) of the solder material. In this study, SAC305 solder was used. Therefore, the reflow temperature was set to 250°C. The specimen was originally 1.5mm thick and reduced to a thickness of approximately 1mm thickness after fabrication by using standard grinding and polishing procedures. Specimens were pre-conditioned for 100 hours at $0.8 \cdot T_{\text{melt}}(\text{K})$, to obtain stable microstructure and to relax

any residual stresses from the reflow or polishing processes. The aging temperature for SAC305 solder was 130°C.

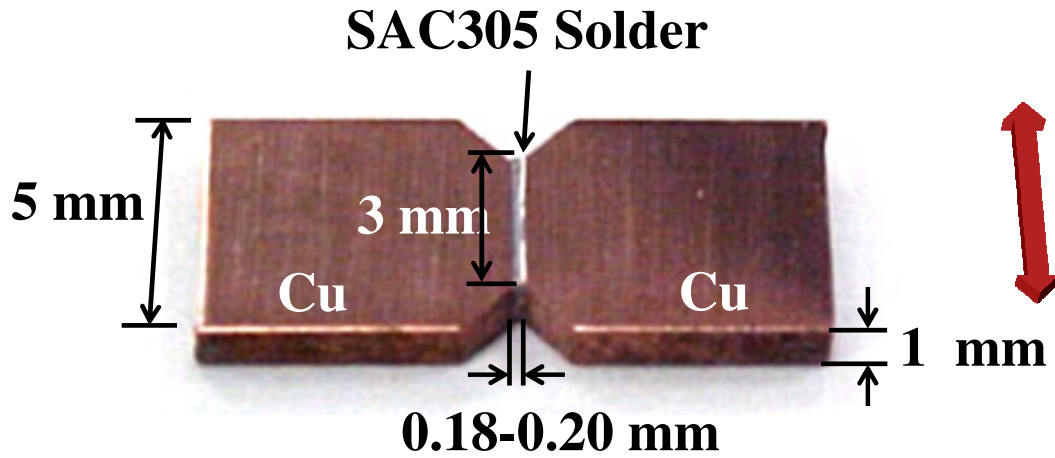


Figure 33. TMM test specimen

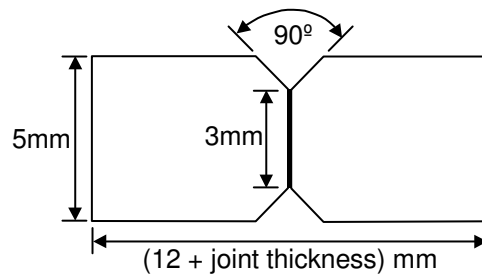


Figure 34. TMM test specimen schematic

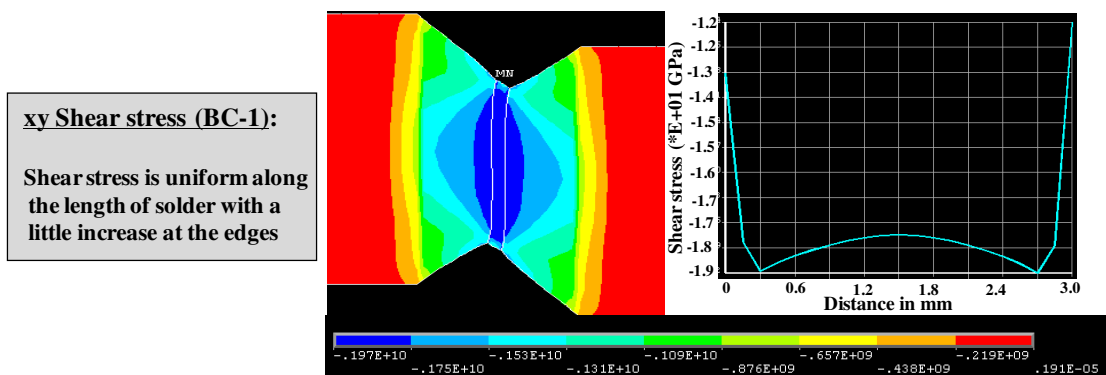
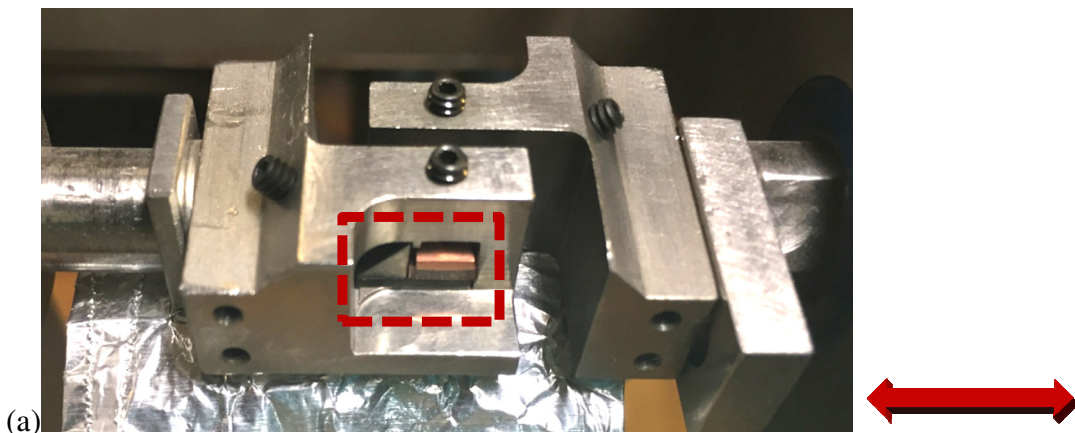


Figure 35. Shear stress distribution in a TMM test specimen [29]

Experimental error was minimized by following procedures such as maintaining consistent fabrication times and methodology and pre-conditioning and pre-test storage conditions (to minimize variations in the dendritic and IMC microstructural features), reduce misalignment of specimen relative to loading and jigs, and sequential screening at various stages of the manufacturing and testing to eliminate defective specimens, to name a few. Each test specimen was individually measured to assess the state of stress as opposed to using nominal solder joint dimensions (3mm length x 1mm thickness x 180 μm wide). Furthermore the storage period from the end of fabrication to start of testing was consistent across all specimens and less than a week to prevent creep degradation resulting from isothermal aging of the SAC microstructure at room temperature. Microstructural image analysis was conducted using optical microscopy and scanning electron microscopy (SEM).

The specimen was mounted on the specimen grips using supporting blocks and locking wedges as shown in Figure 36 (a) and (b). Set screws were used to place the specimen in position.



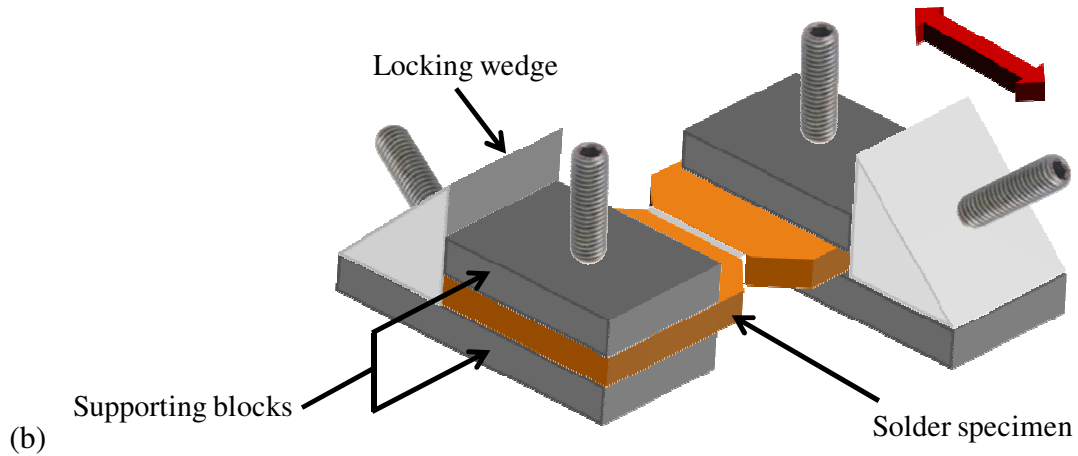


Figure 36. (a) specimen attached to the specimen grips (b) schematic of specimen in grips (red arrow shows the direction of motion of the movable grip)

4.2 Test profiles

The maximum displacement of the TMM actuator is $\pm 45 \mu\text{m}$. Multiple tests were conducted to determine the load levels for the experiments to develop the non-linear damage model. Load levels were finalized to obtain maximum separation of the curves without compromising test duration. The three test profiles are shown in Table XI. All tests were conducted at a constant ramp rate of $10 \mu\text{m/s}$ with no dwell time at both extremes. Ramp rate of $10 \mu\text{m/s}$ and no dwell time were selected to minimize creep effects during cyclic loading. The tests are conducted at room temperature to avoid the additional effects of temperature. The estimation of inelastic strain range for each load is described in detail in Section 4.3.

Table XI. Test profiles.

Test parameters	Load level 1	Load level 2	Load level 3
Initial maximum displacement	+30 μm	+20 μm	+10 μm
Initial minimum displacement	-30 μm	-20 μm	-10 μm
Constant inelastic strain range	0.215	0.107	0.039

The strain ranges tested for the purpose of this dissertation were in the range for high strain-low cycle regime of SAC305 solder. The durability curves for SAC305 solder has been reported by Zhou [30] (see Figure 37).

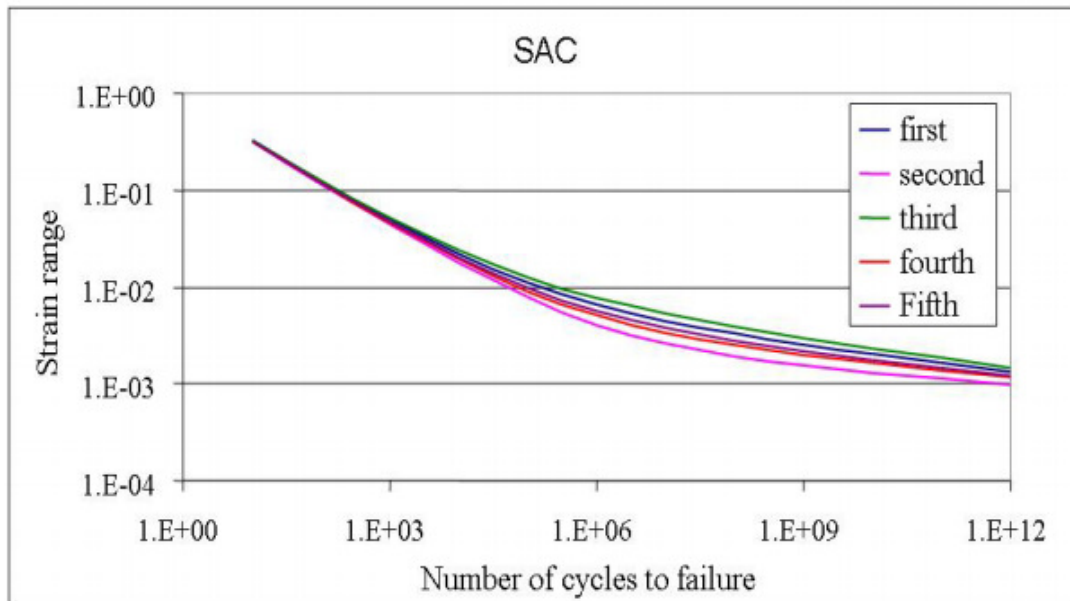


Figure 37. S-N durability curves for SAC solder [30]

To maintain a constant ISR during testing, a cycle update criterion is used real-time in the closed loop. The inputs from the user that defines the initial displacement cycle include maximum and minimum displacements, displacement ramp rates, and upper and lower dwell times. The cycle update criterion is used to determine whether

or not to recalculate and update the control displacement cycle. The adjustment calculation is the method by which the maximum and minimum deformation amplitudes are updated. The cycle update criterion and the adjustment calculation is shown in Figure 38.

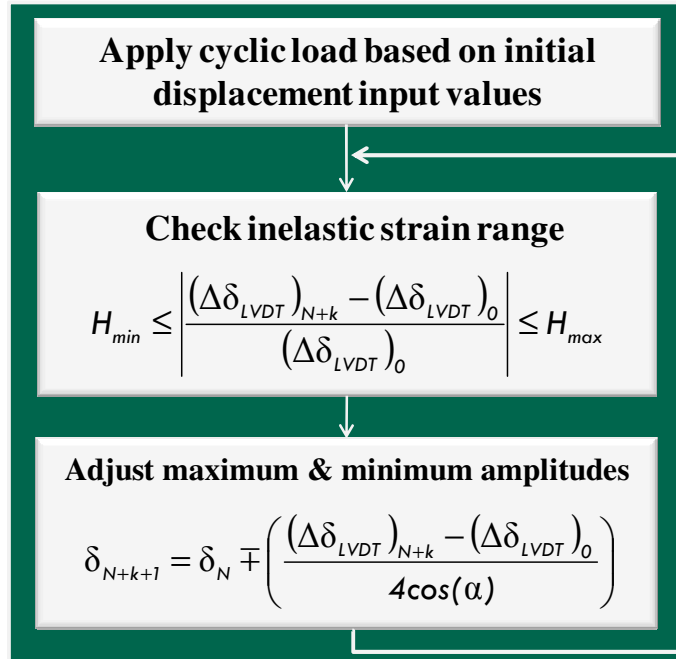


Figure 38. Adaptive inelastic strain range (ISR) controlled testing process including cycle update criterion and adjustment calculation (maximum and minimum amplitudes) [28].

H_{max}/H_{min} : maximum and minimum update criteria

$\Delta\delta_{LVDT}$: LVDT displacement

α : pitch of stress-strain curve at approach to reversal

N : cycle number at which last cycle parameter update occurred

$N+k$: cycle number beyond N at which next parameter update check occurs

$N+k+1$: cycle number using newly updated cycle parameters

0 : initial, baseline cycle

4.3 Interpretation of raw data

The raw data output by the test controller includes the current cycle, elapsed time in seconds, the grip position in microns (from LVDT measurement), and the load in Newton (from load cell). Using these raw data, average engineering shear strain and stress in the solder joint are calculated. The relative displacement provided by the LVDT is the sum of the relative displacements of the grips, solder, and copper platens (see Equation 28).

Equation 28

$$\Delta \delta_{LVDT} = \Delta \delta_{grips} + \Delta \delta_{copper\ platen} + \Delta \delta_{solder}$$

where $\Delta \delta$ is the displacement at respective locations. The compliance of the load train (that is, the specimen grips and the copper platens) is compensated using C_{LT} (measured in $\mu\text{m}/\text{N}$) estimated using FEA analysis. The relative solder displacement is then estimated as (see Equation 29):

Equation 29

$$\Delta \delta_{solder} = \Delta \delta_{LVDT} - PC_{LT}$$

where $\Delta \delta$ is the displacement and P is the instantaneous load measured from load cell. Engineering shear strain (see Equation 30) is calculated based on the relative displacement values from LVDT and solder geometry.

Equation 30

$$\gamma = \frac{\Delta \delta_{solder}}{h} = \frac{\Delta \delta_{LVDT} - PC_{LT}}{h}$$

where γ is the current average shear strain in the solder joint, δ and δ_0 are the current and initial displacements, respectively, P is the current load, C_{LT} is the load train compliance and h is the solder joint height. Engineering shear stress is estimated from load values from the load cell and solder geometry (see Equation 31).

Equation 31

$$\tau = \frac{P}{A_0}$$

where τ is the current average engineering shear stress, P is the current load and A_0 is the original cross-sectional area of the solder joint.

The dimensions of the solder joints of each specimen were measured prior to testing. An average of five solder joint height measurements was considered for strain measurements (see Figure 39).

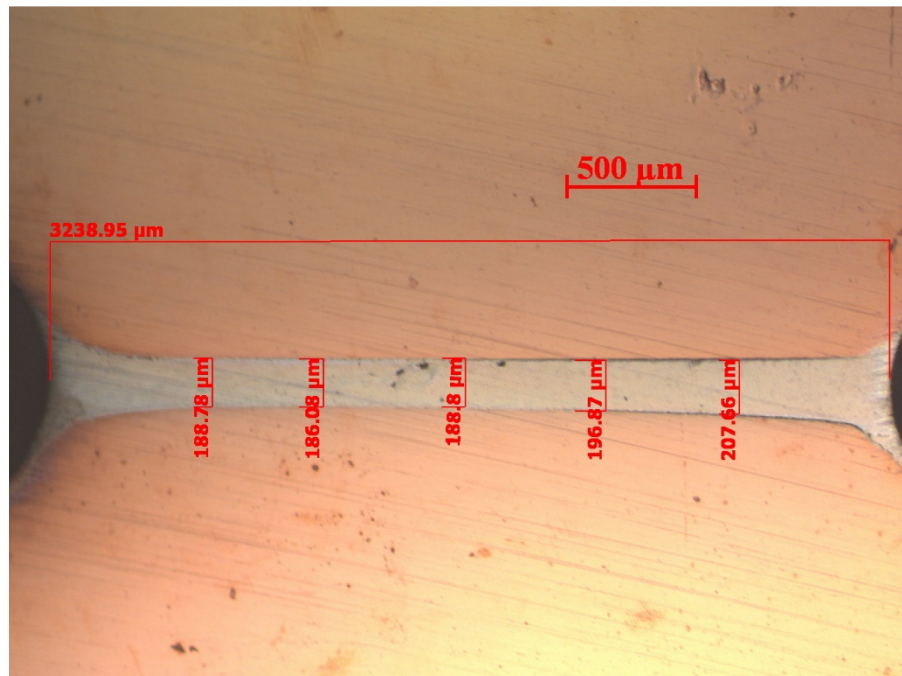


Figure 39. Solder joint height measurements

Mukherjee and Dasgupta [29] conducted a simple two-dimensional elastic-plastic finite element analysis to determine the effects of dimensional variabilities on the shear stress and strain distributions in the solder specimen. Shear stress and strain distributions were estimated using the Ramberg-Osgood model (Equation 32):

Equation 32

$$\varepsilon = \frac{\sigma}{E} + K \left(\frac{\sigma}{E} \right)^n$$

where, ε is equivalent strain, σ is von-Mises stress, E is elastic Young's modulus, K & n are the plastic Ramberg-Osgood constants for the solder considered. The simulations with a non-linear material model showed that the stress in-homogeneities caused due to different variabilities generated during specimen fabrication are smoothed by the plastic deformation occurring in the joint. As an example, the effect of taper on shear stress and strain is shown in Figure 40.

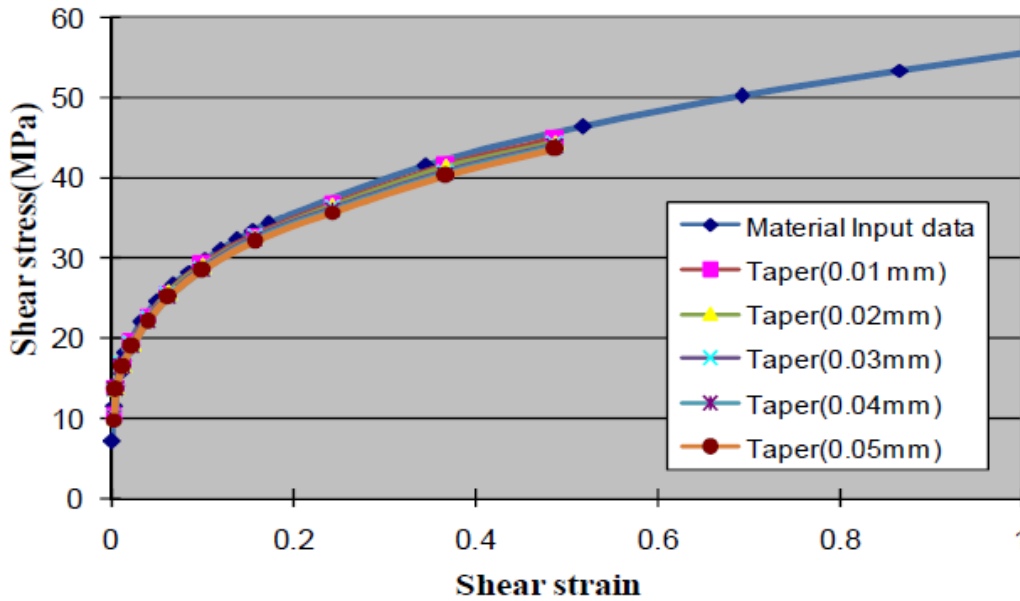


Figure 40. Effect of taper on shear stress and shear strain [29]

From the raw data engineering stress and strain were estimated for each cycle. Five cycles were applied on each specimen to obtain a stable hysteresis loop. The engineering stress-strain from the fifth cycle was considered as the baseline cycle for determining the baseline load range and strain range (see Figure 41).

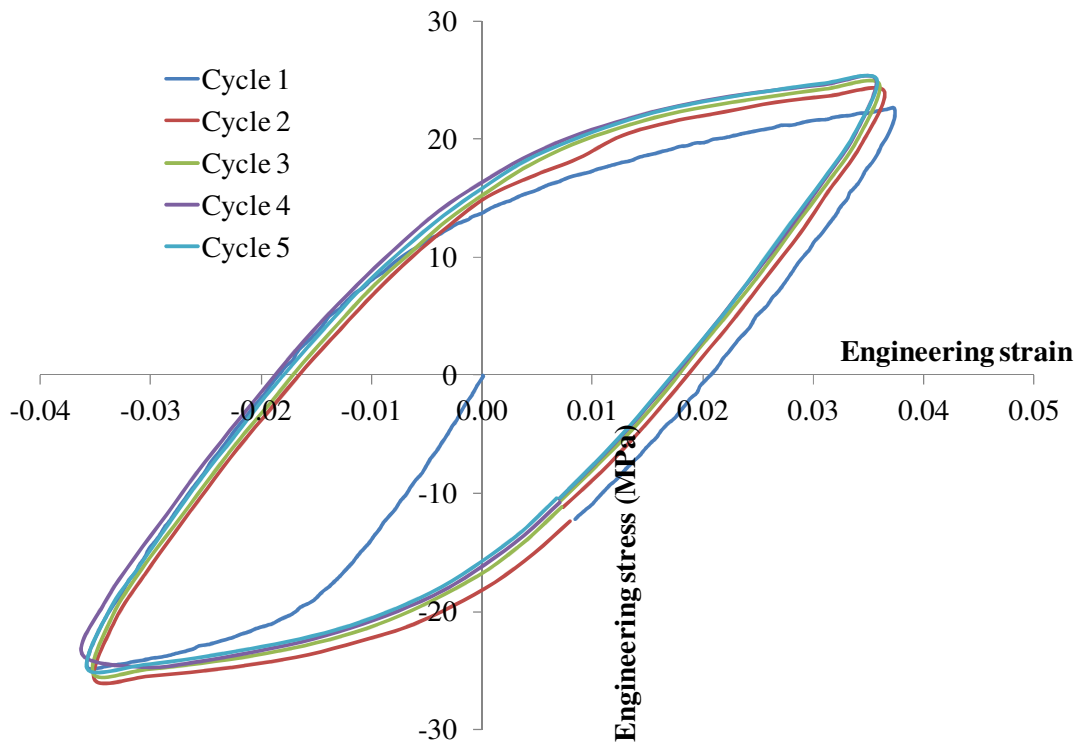


Figure 41. Baseline cycle for the case of load level 3

The total and inelastic strain ranges (TSR and ISR) are determined by the difference of the maximum and minimum strain values per cycle, and the difference of the values of strain at zero stress, respectively. For cases where a discrete data point does not lie exactly upon the strain axis, the zero-stress strain is linearly interpolated between the two closest available data points.

An illustration of the engineering stress-strain of SAC305 solder under load level 3 is illustrated in Figure 42. As mentioned earlier, the hysteresis loop of the fifth cycle was considered as the baseline for the load and strain range estimation, which is

labeled as 0% load drop (blue loop) in Figure 42. The baseline stress range, total strain range and inelastic strain range for load level 3 were approximately 50 MPa, 0.071, and 0.035 respectively.

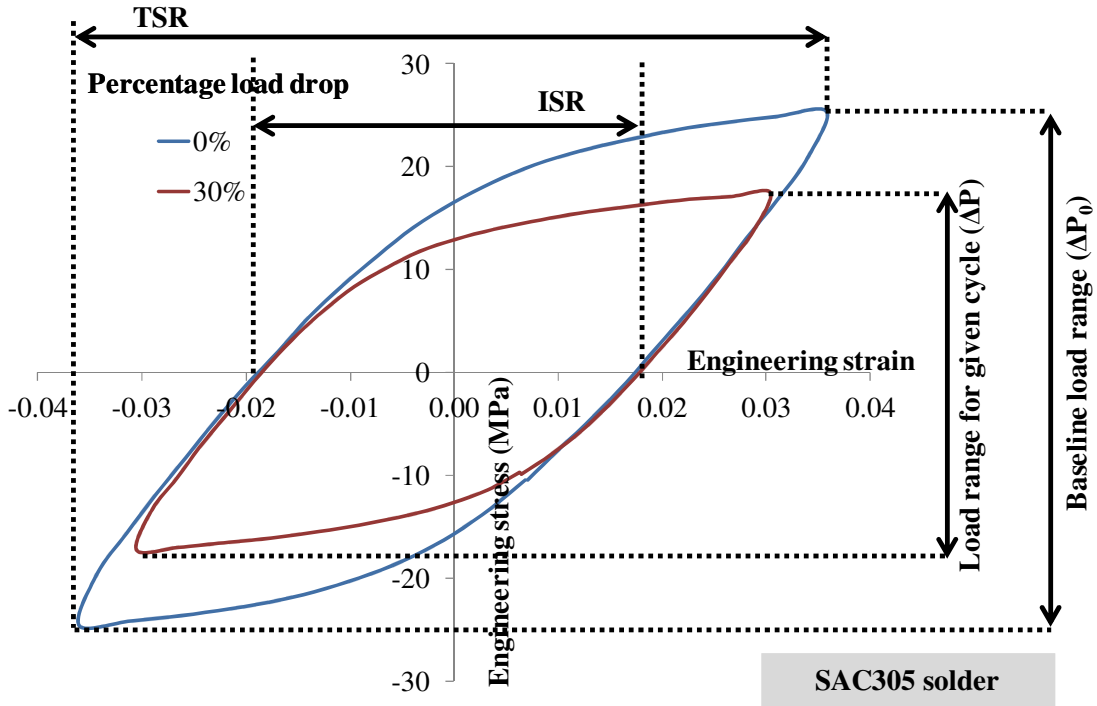


Figure 42. Hysteresis loop during inelastic strain range controlled cyclic test (load level 3)

Load drop is defined as the ratio of the change in load from baseline load to the baseline load (see Equation 33). Load drop is widely used as a failure criterion for cyclic mechanical tests since a drop in the baseline load level denotes a drop in the load bearing capacity of the solder joint. Although 50% load drop is commonly used, since our objective was to obtain maximum life during the crack propagation phase the failure of a specimen was defined as 80% load drop from the baseline load. A limitation of the experimental test setup prohibited further drop in load beyond 80%.

Equation 33

$$L.D. = \frac{\Delta P_0 - \Delta P}{\Delta P_0}$$

where ΔP is the stress/load range.

The drop in load bearing capacity of the capacity until 80% load drop under load level 3 for SAC305 solder is shown in Figure 43. With the progressive drop in load during ISR controlled test, the applied displacement range is constantly updated to maintain a constant value of inelastic strain range during the cyclic test.

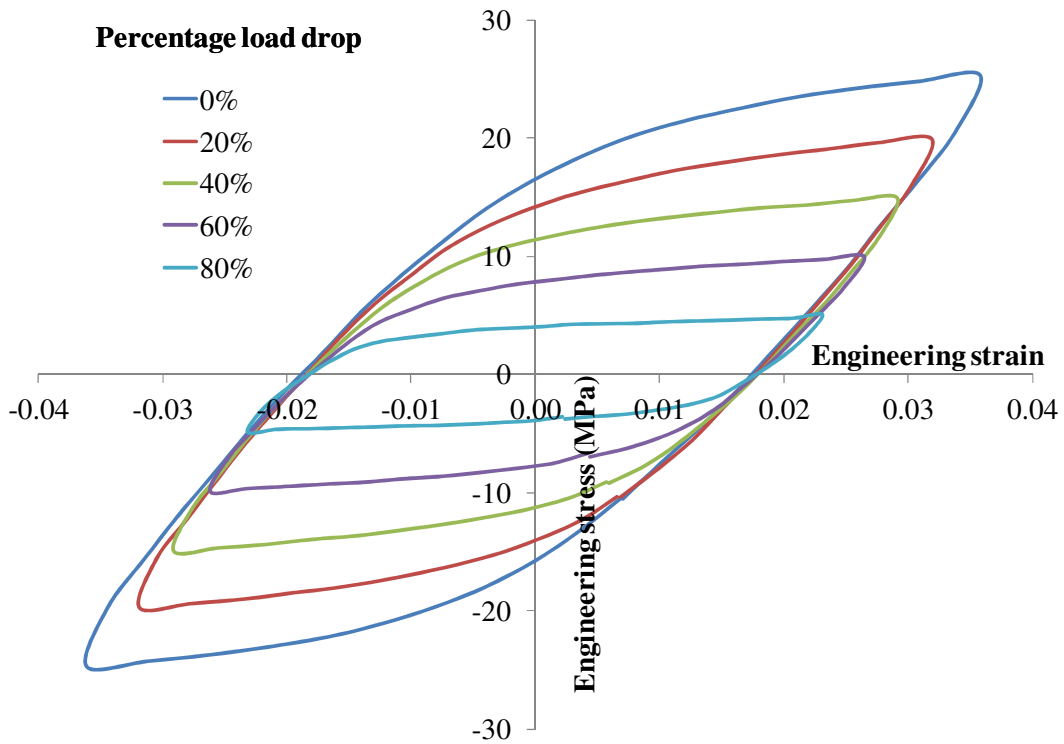


Figure 43. Drop in load during constant inelastic strain range controlled test (load level 3).

Figure 44 shows that the inelastic strain range is held constant during the entire duration of the test.

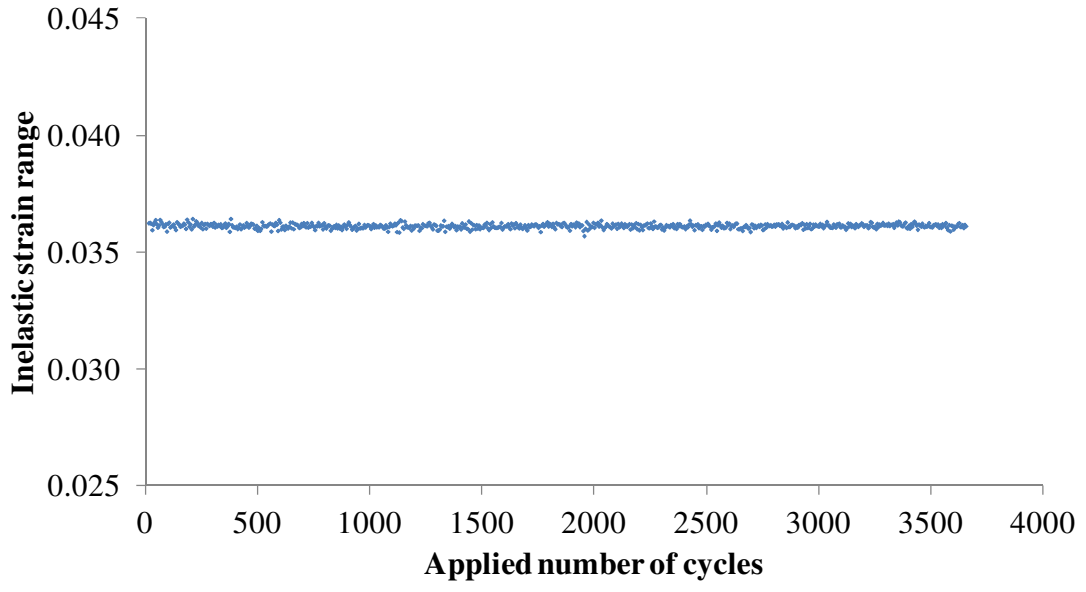


Figure 44. Inelastic strain range during test

Chapter 5: Load-dependent Non-Linear Damage Model

5.1 Derivation of the form of non-linear damage model

The damage accumulation in solders was considered analogous to crack propagation to determine the form of the non-linear damage model. In a solder material, the microcracks nucleate and grow at the grain boundaries under cyclic loading. These microcracks eventually link-up to form one or more macrocracks resulting in the failure of the solder interconnect. One of the most widely used crack propagation laws to represent macrocrack propagation is Paris' law (see Equation 34) [31].

Equation 34

$$\frac{da}{dN} = A(\Delta K)^m$$
$$\Delta K = \Delta\sigma Y \sqrt{\pi a}$$

where a is the crack length, N is the applied cycles, ΔK is the stress intensity factor, A and m are fitted parameters based on material, $\Delta\sigma$ is the load range, and Y is a parameter dependent on the geometry. In this section, the form of the non-linear damage model is derived from the Paris' crack propagation law. Integration of the Paris' crack equation (Equation 34) provides the number of cycles required to reach a specific crack length (see Equation 35).

Equation 35

$$\int dN = \frac{1}{A(\Delta\sigma Y \sqrt{\pi})^m} \int a^{-\left(\frac{m}{2}\right)} da$$

For the sake of simplicity, the damage due to crack initiation is ignored in this step and it is assumed that Paris' law is valid from the beginning of load application until failure. If the length of the crack is a_n at 'n' number of applied cycles, then integration of the Paris' law provides a relationship between applied number of cycles and instantaneous length of crack at cycle 'n' (see Equation 36).

Equation 36

$$n_p = \frac{1}{A(\Delta\sigma Y \sqrt{\pi})^m} \left[\frac{a^{-\left(\frac{m}{2}\right)+1}}{-\left(\frac{m}{2}\right)+1} \right]_0^{a_n}$$

If failure occurs when the crack length reaches a critical crack length (a_c), integration of the Paris' law provides the relationship between the cycles to failure and critical crack length (see Equation 37).

Equation 37

$$N_f = \frac{1}{A(\Delta\sigma Y \sqrt{\pi})^m} \left[\frac{a^{-\left(\frac{m}{2}\right)+1}}{-\left(\frac{m}{2}\right)+1} \right]_0^{a_c}$$

For the same loading condition, dividing Equation 36 by Equation 37 provides the cycle ratio with respect to the cycles to failure (see Equation 38).

Equation 38

$$\frac{n_p}{N_f} = \frac{a_n^{-\left(\frac{m}{2}\right)+1}}{a_c^{-\left(\frac{m}{2}\right)+1}} = \frac{(a_n/a_c)^{-\left(\frac{m}{2}\right)+1}}{1}$$

Taking damage $D_p=a_n/a_c$, the relationship between cycle ratio and damage is given in the following form (see Equation 39):

Equation 39

$$\frac{n_p}{N_f} = D_p^{-\left(\frac{m}{2}\right)+1}$$
$$D_p = \left(\frac{n_p}{N_f}\right)^{\frac{2}{(2-m)}}$$

The total damage is defined as the damage due to crack initiation and damage due to crack propagation. If we assume that Paris's law is applicable in the crack initiation phase, then the following form of damage equation is obtained (see Equation 40).

Equation 40

$$D_n = D_i + D_p$$
$$D_n = D_i + \left(\frac{n_p}{N_f}\right)^{\frac{2}{(2-m)}}$$
$$D_n = \left(\frac{n_i}{N_f}\right)^{\frac{2}{(2-m)}} + \left(\frac{n_p}{N_f}\right)^{\frac{2}{(2-m)}} = \left(\frac{n_i}{N_f}\right)^{\frac{2}{(2-m)}} + \left(\frac{n - n_i}{N_f}\right)^{\frac{2}{(2-m)}}$$

where D_0 is the initial damage and considered as crack initiation damage according to Paris' law. According to Paris' law ' m ' is a parameter dependent on the material. However, the dependence of ' m ' on the applied load level has been demonstrated by Benachaour [32] for steel specimens. Further, damage accumulation is considered to be a function of the applied load level to take into account the effect of load sequence. Therefore, the exponent ' m ' in Paris' equation must be a function of the applied load level. Therefore, based on the derivation from Paris' law the form given in Equation 41 was pursued for the non-linear damage model.

Equation 41

$$D_n = \left(\frac{n_i}{N_f} \right)^{\text{damage exponent}} + \left(\frac{n - n_i}{N_f} \right)^{\text{damage exponent}}$$

5.2 Development of damage curves at different load levels

To experimentally develop the damage exponents at different load levels, a suite of tests were carried out at single level cyclic loading conditions and sequential loading conditions until failure. Tests at single level cyclic loading condition were conducted to determine the cycles to failure under a particular loading condition (N_f). Three sets of sequential loading tests were required to experimentally determine the damage exponents at three load levels. Tests 1 through 3 are carried out to determine N_f and tests 4, 5, and 6 were carried out to develop damage curves. Three samples were tested for each test condition to obtain a statistical spread on the data. Remaining tests were carried out to validate the developed constants of the non-linear damage model.

The average cycles to failure and the standard deviation for the single level cyclic and sequential tests are provided in Figure 45. The severity of the applied load

decreased from load level 1 to load level 3. Therefore, the cycles to failure for the single level cyclic tests increased from load level 1 through load level 3.

No.	Test profiles	Load level	Average cycles to failure	Standard deviation	Sample size
1	Load level 1 until failure	1	338	12%	3
2	Load level 2 until failure	2	1501	8%	3
3	Load level 3 until failure	3	3238	19%	3
4	Load level 1 (until 30% load drop) followed by Load level 2 until failure	1	119	10%	3
		2	1219	21%	
5	Load level 1 (until 60% load drop) followed by Load level 2 until failure	1	176	14%	3
		2	1060	10%	
6	Load level 1 (until 30% load drop) followed by Load level 3 until failure	1	79	18%	3
		3	2931	20%	

Figure 45. Average cycles to failure under different test profiles.

Equation 25 and Equation 26 were modified to include the effect of damage due to crack initiation (see Equation 42). For the purpose of this dissertation the damage due to crack initiation was assumed to 10% of the total life of the first applied load level. Also, it is assumed that the applied number of cycles in the first load level (n_1) is greater than that due to crack initiation (n_i). In other words, it is assumed that the crack has already initiated after the application of the first load level and the crack is in the propagation phase in the subsequent load levels. Equation 42 and experimental results from Figure 45 were used to develop damage exponents for load levels 1, 2, and 3.

Equation 42

$$1 = \left(\frac{n_i}{N_{f_1}} \right)^{F(N_{f_1})} + \left(\frac{n_1 - n_i}{N_{f_1}} \right)^{F(N_{f_1})} + \left(\frac{n_2}{N_{f_2}} \right)^{F(N_{f_2})}$$

The numerical values of the damage exponents for load levels 1, 2, and 3 were 1.05, 1.76, and 2.69 respectively. The corresponding damage curves for these load levels are shown in Figure 46. The numerical values of damage exponents decreased as the load level became harsher. This follows the hypothesis described earlier in chapter 2.

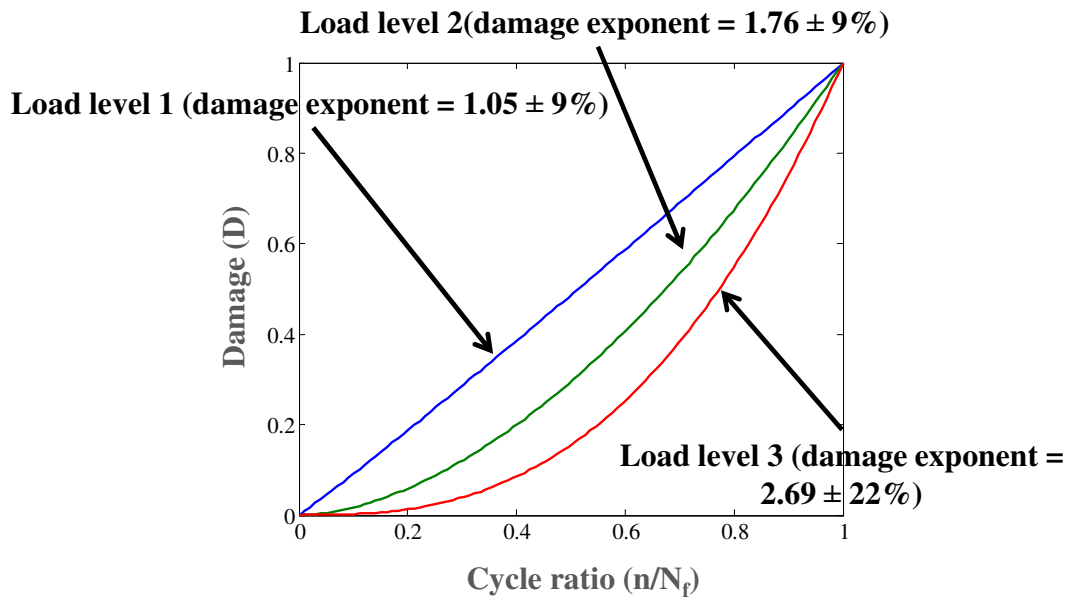


Figure 46. Damage curves for load levels 1, 2, and 3

5.3 Validation of non-linear model

To validate the experimentally determined damage exponents, tests were conducted under a new loading condition and in reverse sequence.

5.3.1 Validation of damage exponents (under new loading condition)

Specimens were subjected to 60% load drop under harsh load level followed by mild load level until failure. As seen in Table XII, the remaining cycles to failure under the mild load level predicted by Miner’s rule was significantly greater than the experimental cycles to failure. On the other hand, the non-linear damage model predictions for both specimens were close to the experimental cycles to failures.

Table XII. Comparison of non-linear model and Miner’s rule predictions to experimental results under new loading condition.

No.		7	
Sample		7A	7B
Test profiles		Load level 1 (106 cycles) followed by load level 3 until failure	Load level 1 (140 cycles) followed by load level 3 until failure
Experimental cycles to failure		950	775
Remaining life under second loading	Miner’s rule prediction	2222	1896
	% error	134%	145%
	Model prediction (average)	1174	938
	% error (average)	23%	21%

5.3.2 Validation of damage exponents (under reverse load sequence)

To demonstrate that the developed damage exponents are valid in the reverse loading sequence, three sets of tests were carried out: medium-harsh sequence, mild-medium sequence, and mild-harsh sequence. As reported in Table XIII, the non-linear damage model accurately predicted the remaining cycles to failure under the second load level. A comparison of the non-linear model prediction to that of Miner's rule showed that the non-linear model prediction had lower percentage errors than Miner's rule.

Table XIII. Comparison of non-linear model and Miner's rule predictions to experimental results under reverse loading sequence.

No.		8	9	10
Test profiles		Load level 2 (274 cycles) followed by load level 1 until failure	Load level 3 (1522 cycles) followed by load level 2 until failure	Load level 3 (1056 cycles) followed by load level 1 until failure
Experimental cycles to failure		315	1183	266
Remaining life under second loading	Miner's rule prediction	277	813	227
	% error	12%	31%	15%
	Model prediction	307-327	865-1209	294-330

No.		8	9	10
	(range)			
	% error	-2.4% to 3.8%	-26.9% to	10.8% to
	(range)		2.3%	24.2%

5.4 Relationship between damage exponent and applied load level

The relationship between damage exponent and the applied load level has been derived in Equation 40. Based on the experimentally developed damage exponents, the numerical values of load dependent Paris' law exponent (m) is developed. A logarithmic model (see Equation 43) provided the best regression fit between Paris exponent (m) and cycles to failure (N_f). The developed exponents are provided in Figure 47.

Equation 43

$$\text{damage exponent} = F(N_f) = \frac{2}{2-m} = \frac{2}{2-(a \ln(N_f) + b)}$$

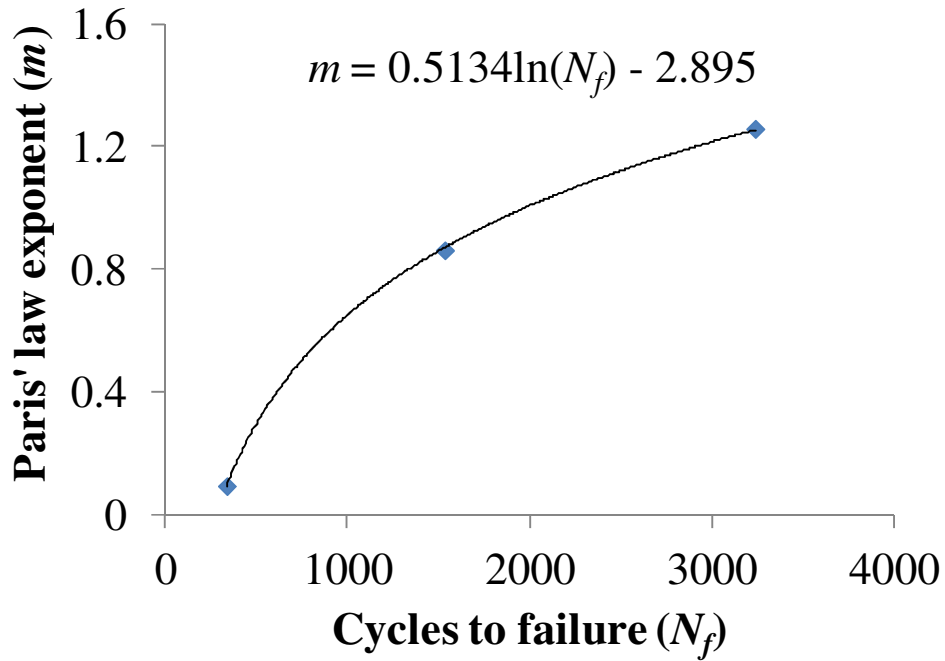


Figure 47. Relationship between Paris' law exponent (m) and cycles of failure of the applied load level

On the other hand, a linear model provided the best regression fit between Paris exponent (m) and cycles to failure (N_f) (see Equation 44). The developed exponents are provided in Figure 48.

Equation 44

$$\text{damage exponent} = F(N_f) = \frac{2}{2-m} = \frac{2}{2-(a \times \text{ISR} + b)}$$

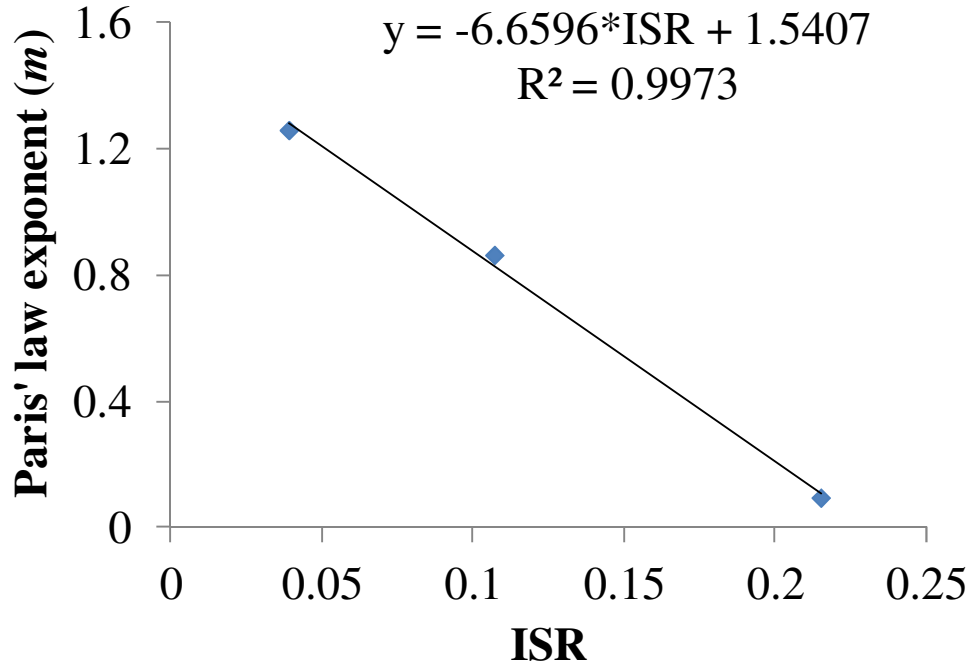


Figure 48. Relationship between Paris' law exponent (m) and cycles of failure of the applied load level

The non-linear damage model for SAC305 solder under sequential loading conditions (see Equation 45) is given as:

Equation 45

$$D_n = \left(\frac{n_i}{N_f} \right)^{\frac{2}{2-(a \ln(N_f)+b)}} + \left(\frac{n - n_i}{N_f} \right)^{\frac{2}{2-(a \ln(N_f)+b)}}$$

where n_i is the cycles to crack initiation, n is the cycles under the applied loading condition and N_f is the cycles to failure under that load level. Model constants, a and b , are dependent on the solder material and were estimated to be 0.5134 and -2.895 respectively for SAC305 solder.

To determine the effect of the assumption that cycles to crack initiation is 10% of the total cycles to failure, a sensitivity analysis was carried. The ratios of the crack

initiation cycles were varied from 5% to 20% and the corresponding damage exponents for the three load levels are shown in Table XIV. It was observed that the damage exponents did not vary significantly with the change in crack initiation cycles.

Table XIV. Sensitivity of damage exponents to the change in percentage initiation

% damage initiation	Damage exponents		
	Load level 1	Load level 2	Load level 3
5%	1.05	1.79	2.71
10%	1.05	1.76	2.69
15%	1.06	1.72	2.66
20%	1.08	1.64	2.65

5.5 Physical explanation of damage curve model

In eutectic tin-lead solder, the microcracks nucleate and grow at the Sn-Sn grain boundaries and Sn-Pb phase boundaries under cyclic loading. These microcracks eventually link-up to form one or more macrocracks resulting in the failure of the solder interconnect. The microstructure of a polycrystalline material can be regarded as a network of discrete interconnected elements, such as phases or grains. A node connected to its neighbor by a link replaces each phase or grain. The lattice approximation of a polycrystalline material into nodes and links is shown in Figure 49. The presence or absence of a link represents either an intact or cracked grain or interphase boundary. The microcrack growth propagation is explained using percolation theory which studies the effects of random disorder. The random disorder

includes missing links in a system, such as lattices which are either random or ordered. In the lattice approximation of polycrystalline materials, the percolation threshold occurs when an infinite array of missing links appear. The corresponding situation in a solid saturated with microcracks is when the microcracks link up to form a macrocrack and is defined as conductivity percolation. The use of percolation theory is justified when the main source of damage is microcrack nucleation at the grain or interface boundaries. Stolkarts et al. showed that for eutectic tin-lead solder, the damage is primarily due to microcrack nucleation at the grain or interface boundaries and hence percolation theory was applied [33].

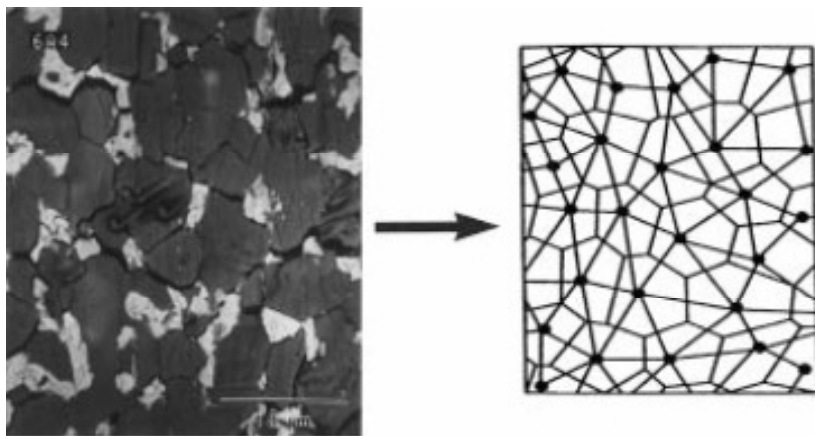


Figure 49. Lattice approximation of a polycrystalline material [33]

The density of microcracks increases with continued cycling and percolation theory is used to estimate the microcrack density at the applied number of cycles. Failure of the solder joint occurs when the microcrack density reaches the percolation threshold. In strain-controlled experiments, the percolation threshold is characterized by the decline in peak stress. The microcrack density at any cycle of fatigue loading is directly proportional to the applied number of cycles. Stolkarts et al. also showed that

for eutectic tin-lead solder, the damage evolution showed power law dependence to the lifetime [33].

Similar to eutectic tin-lead solder, the microcracks nucleate at recrystallized areas or regions with fine grains or high density of grain boundaries in lead-free solders [34]. Hence, the percolation theory can be applied to lead-free solders to explain the microcrack nucleation and accumulation. Wen et al. [21] used percolation theory to model damage evolution in eutectic Sn3.5Ag solder. Using percolation theory a power law relationship was established between damage and ratio of applied number of number to cycles to failure. This provides a physical explanation to the power law equation used in the damage curve methodology.

Failure analysis was carried out on one failed specimen from each test level to confirm that failure was due to fatigue fracture in the SAC305 solder. The specimens were inspected in an environmental scanning electron microscope (ESEM) for the presence of cracks. In all the inspected specimens, cracks were observed in the bulk solder and continued along the solder/copper interface. The failure site in a specimen subjected to a sequential loading condition is shown in Figure 50. Locations of failure sites for other test cases are provided in **APPENDIX B: Failure Analysis**.

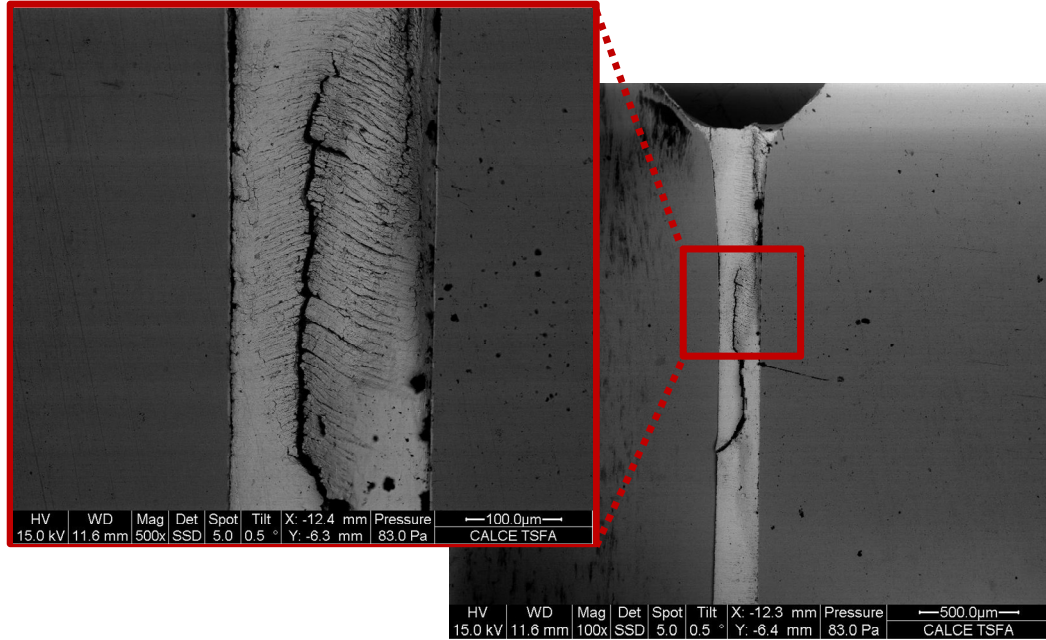


Figure 50. Failure site in a test specimen subjected to load level 1 followed by load level 3 until failure

To determine if the crack propagation was along the grain boundaries during the application of cyclic loading, cross polarized images were taken on the samples prior to testing. The cross polarized images were taken using Nikon Eclipse LV100POL. The inspection of a specimen prior to application of any cyclic loading showed the presence of large tin grains (see Figure 51). The tin grain structure is similar to that of the TMM test specimen reported by Cuddalorepatta and Dasgupta [35].

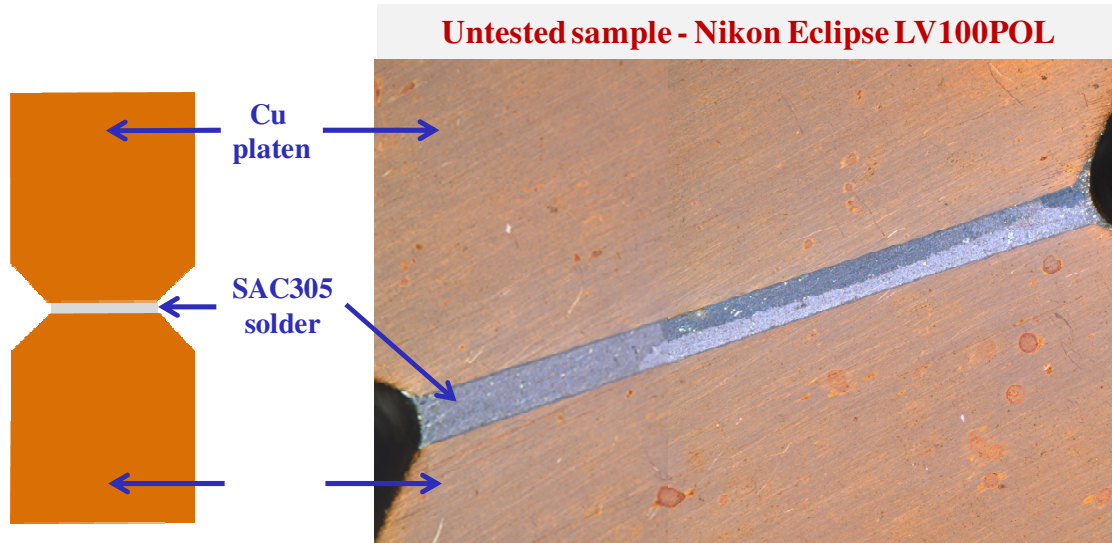


Figure 51. Tin grains in untested SAC solder specimen

The specimen shown in Figure 51 was subjected a sequential loading case of load level 1 (load drop of 60%) followed by load level 3 until failure. Inspection of the failed specimen under ESEM revealed that the crack propagation was along the tin grain boundary and the solder interface (see Figure 52). Analysis revealed the presence of significant damage of the solder material along the tin grain boundary.

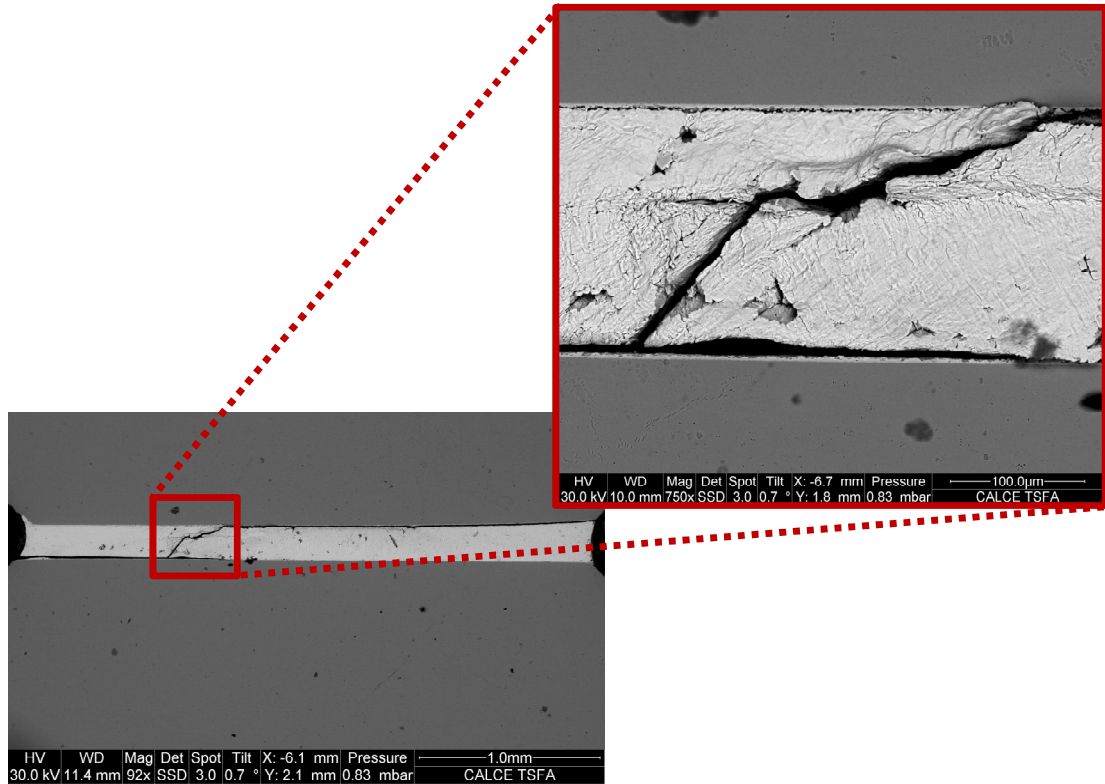


Figure 52. Crack propagation along the tin grain boundary

5.6 Miner's rule vs non-linear damage model

Based on the experimental data, a comparison of the Miner's rule and non-linear damage model shows that damage estimated using Miner's rule may provide reasonable results in certain cases. These cases include:

1. A milder load level followed by a harsher load level: As evident from Table XIII when a milder load level is applied followed by a harsher load level, the Miner's rule prediction provides predictions close to the experimental cycles to failure. This may be due to the fact that there is not sufficient damage accumulated during the mild loading condition such that the life under the harsh loading condition is affected. Therefore, the majority of the damage occurs during the harsh load level.

2. Minimal separation between load levels: If the load levels applied under in a sequential fashion are close to each in magnitude, the non-linear damage model approximately reduces to a linear model. For instance, when the load levels are close to each other, the ratio of the numerical values of the damage exponents will be approximately equal to 1. In that case, Equation 22 and Equation 23 would reduce to Miner's rule. Therefore, Miner's rule and non-linear damage model would provide approximately the same remaining life predictions.
3. The magnitude of the applied load level is in the ISR range of load level 1: The numerical value of the damage exponent for the load level is close to 1. Therefore, in such a case, the non-linear damage model reduces to Miner's rule.

5.7 Limitations of the non-linear damage model

The developed non-linear damage model is limited to use for cyclic loading conditions. Cyclic loads are defined as the application of repeated or fluctuating strains/stresses involving load reversals. Therefore, the proposed model is applicable to non-cyclic loading conditions, such as monotonic loading or aging conditions.

The non-linear damage model presented in this dissertation was developed based on material level testing under cyclic shear testing at room temperature. Therefore, based on the model constants developed in this dissertation, the applicable load types is limited to cyclic shear loads at room temperature. This model considers only the damage due to time-independent inelastic (plastic) strain. In the current form, this non-linear model does not take into account the damage due to time dependent

inelastic (creep) strain. The effect of temperature on the model constants has not been documented in this dissertation. To broaden the scope to other load types, such as temperature cycling and mechanical bend cycling, further testing is required. The methodology presented in this dissertation is generic in nature; therefore conducting experiments at other load types will enable the development of model constants for various other loading types. However, inclusion of damage due to creep may require inclusion of additional parameters or even modification of the form of the damage model.

The model is developed for cyclic loading with zero mean stress/strain. Therefore, the impact of the change in mean stress/strain has not been evaluated and characterized in the current form of the non-linear damage equation.

The current model has been validated for SAC305, which is the de-facto lead-free solder. For other solder materials, further testing may be required to develop new model constants.

The form of the non-linear model is based on the assumption that Paris' crack growth law is valid for cyclic shear loads under room temperature conditions. Additionally, there are two assumptions that have not been validated. First, the damage due to crack initiation is assumed to be 10% of the cycles to failure under a particular load level. Although, it has been shown that the damage exponents did not vary significantly with the change in the damage due to crack initiation from 5% to 20%, there is a need for accurate estimation of the cycles to crack initiation. The damage due to crack initiation can be experimentally determined by continuous/periodic monitoring of the solder specimen during cyclic loading. Second,

for the purpose of this dissertation, it is assumed that Paris' law is valid during the crack initiation phase since there are no existing models to incorporate the damage due to crack initiation in terms of cycle ratio.

For the experimental determination of damage exponents there is an inherent assumption that the damage is proportional to the load drop. The damage exponents and model constants are valid for the case of a failure criterion of 80% load drop. Although 70% load drop did not significantly change the values of damage exponents (Appendix D), the variation in damage exponents with respect to other values of load drop has not been quantified. Additionally, if a different failure criterion is used, for instance, resistance change, the damage exponents may be impacted.

Although the proposed non-linear model has limitations, this dissertation provides a general methodology to develop non-linear damage curves for solder interconnects under sequential cyclic loading conditions. The applicability of this general methodology needs to be tested and validated for different cases in future studies.

Chapter 6: Dissertation Contributions

The contributions of this dissertation are:

- Proposed and developed a non-linear damage model with load-dependent damage exponents that takes into account the sequence effect under sequential cyclic loading conditions.
 - Provided an approach to experimentally determine load dependent damage exponents under sequential cyclic loads.
 - Developed an analytical relationship between the damage exponent and the applied load level as defined by cycles to failure (N_f) based on Paris' crack growth law.
- Validated the non-linear damage model for SAC305 solder.
 - Determined load dependent Paris' law exponents for SAC305 solder.

Chapter 7: Future Work

The load-dependent non-linear damage model developed in this dissertation has been validated only for SAC305 solder. The coefficients developed in the analytical relation between damage exponent and load level are dependent on the type of solder material. Therefore, if the experimental approach proposed in this dissertation is carried out for any new solder, the material determined coefficients can be established.

The proposed model has been developed for high strain–low cycle loading conditions. The validity of the model in the low strain–high cycles loading conditions is yet to be determined. An additional extension of the model is to include different load types in addition to the different load levels. This may require modification of the existing form of the non-linear model or inclusion of additional coefficients to incorporate the load type effect. For instance, to consider temperature cycling load type, damage due to creep (time dependent inelastic damage) must be taken into account in addition to the plastic damage (time independent inelastic damage).

The proposed model assumes the damage due to crack initiation to be a constant regardless of the applied load level. However, that may not be the case in real life scenarios. Therefore, the accuracy of the model may be improved by developing test methodologies to monitor crack initiation and propagation in situ. This will enable clear distinction of the damages due to crack initiation and propagation.

The model developed in this dissertation is based on testing in TMM and therefore is independent of the solder geometry. The effect of component geometry may be included to provide more practical applicability to the developed model.

APPENDIX A: Analytical Relation from Experimental Fit

An analytical relation between the damage exponent and applied load level was developed without considering the form derived from Paris's law of crack propagation. A linear form provided the best fit (highest R^2) to the experimental data. The form of the damage exponent is given in Equation 46.

Equation 46

$$\text{damage exponent} = F(N_f) = a \times N_f + b$$

The damage exponent and cycles to failure follow the relationship as shown in Figure 53 and the developed power law coefficients are provided in Table XV.

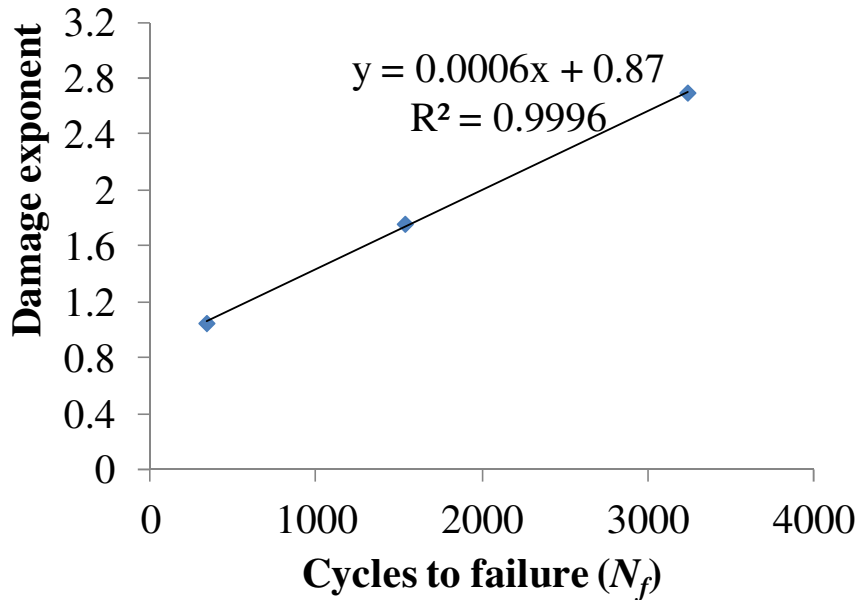


Figure 53. Relationship between damage exponent and cycles to failure.

Table XV. Coefficients from experimental data

	a	b
Coefficient	0.0006	0.87

APPENDIX B: Failure Analysis

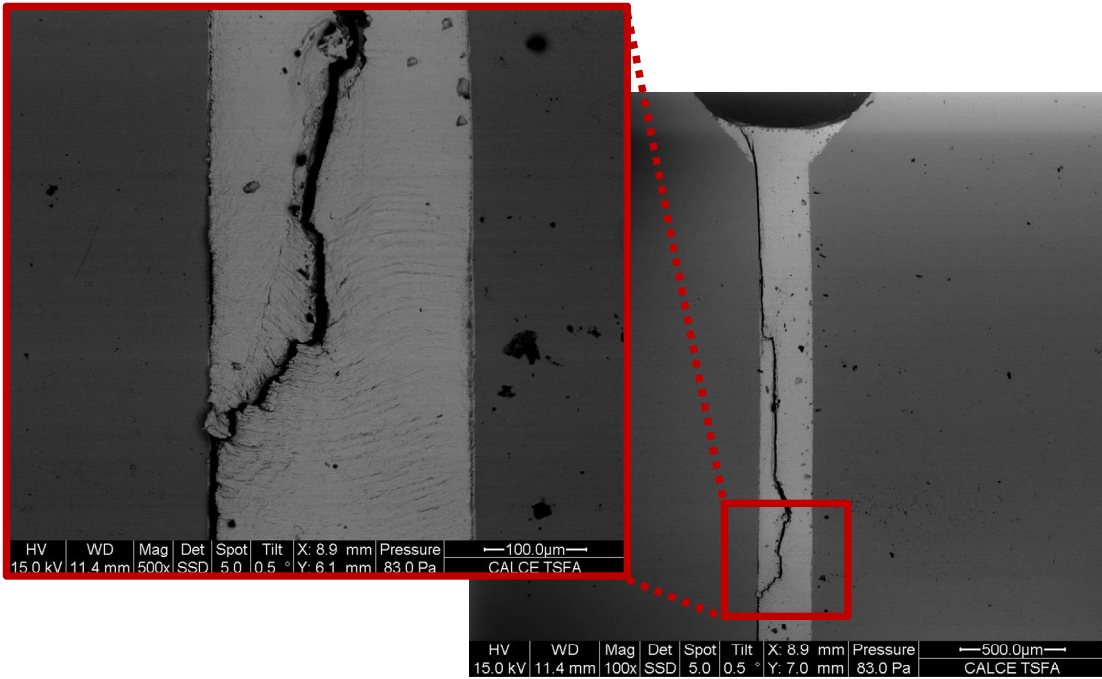


Figure 54. Failure site in a test specimen subjected to load level 2 until failure

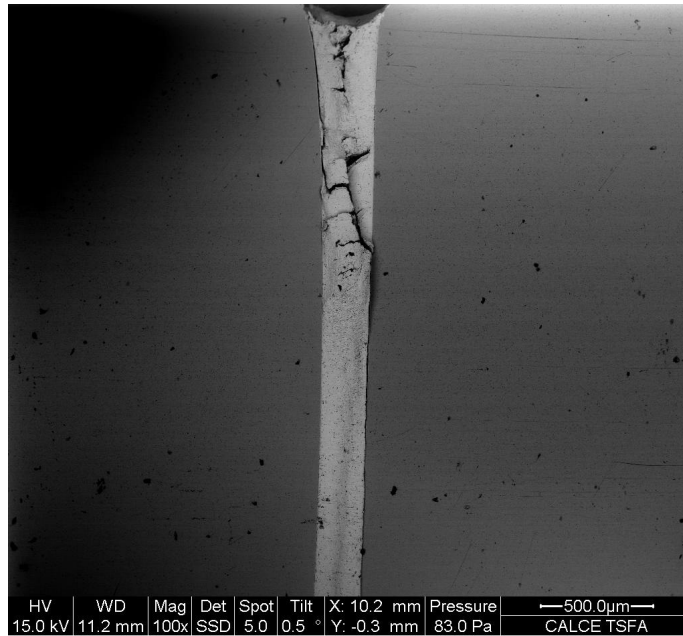


Figure 55. Failure site in a test specimen subjected to load level 1 until failure

APPENDIX C: Load Drop for Load Levels 1, 2, and 3

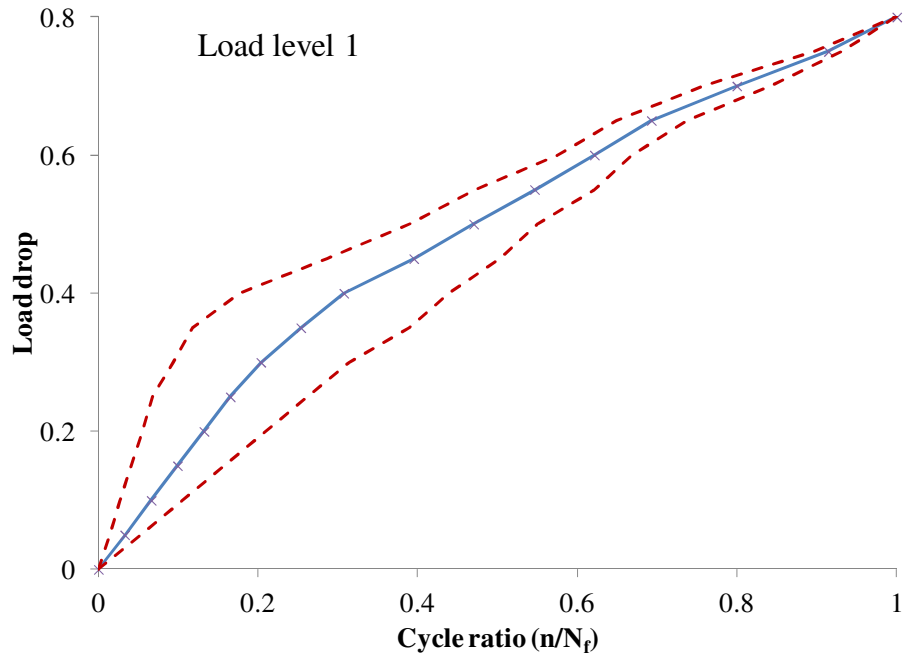


Figure 56. Average load drop under load level 1 (bounds = one standard deviation)

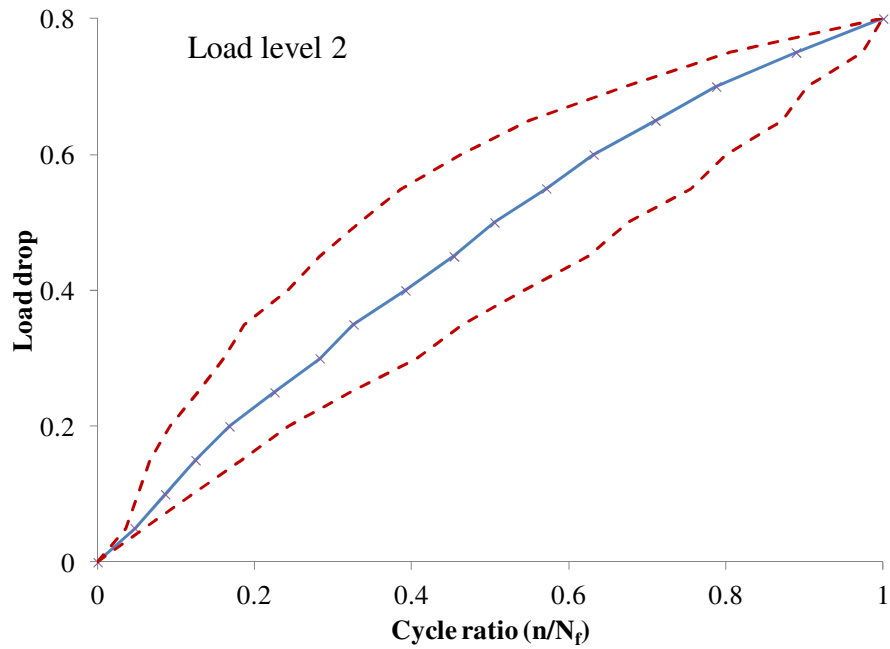


Figure 57. Average load drop under load level 2 (bounds = one standard deviation)

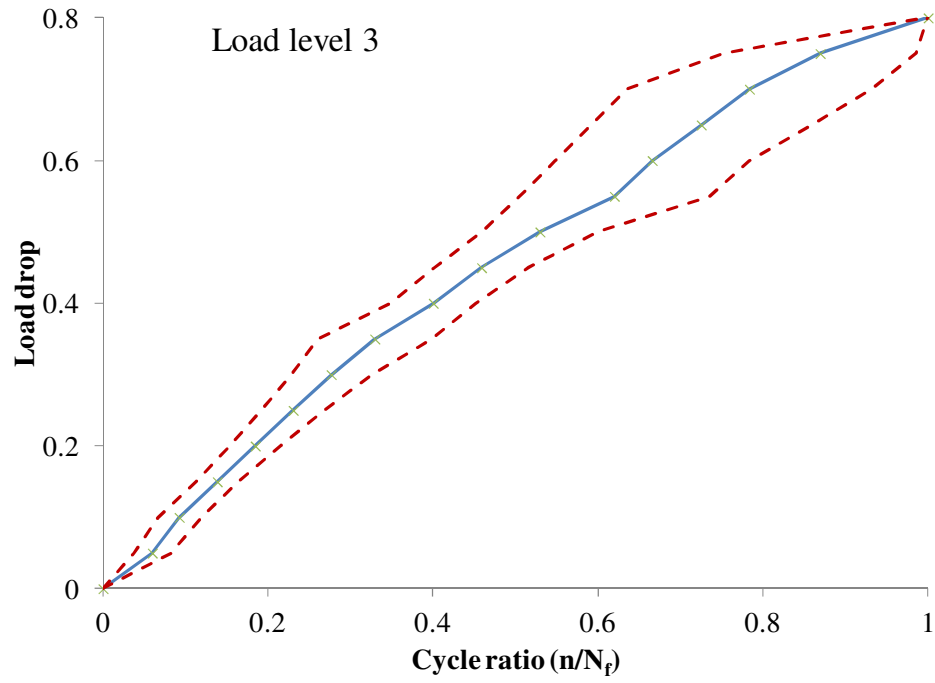


Figure 58. Average load drop under load level 3 (bounds = one standard deviation)

APPENDIX D: Sensitivity of Failure Criterion

In order to determine the sensitivity of the failure criterion, damage exponents were determined using a failure criterion of 70% load drop. A comparison of 70% and 80% load drop did not show a significant variation in the numerical values of the experimentally determined damage exponents (see Figure 59 and Table XVI).

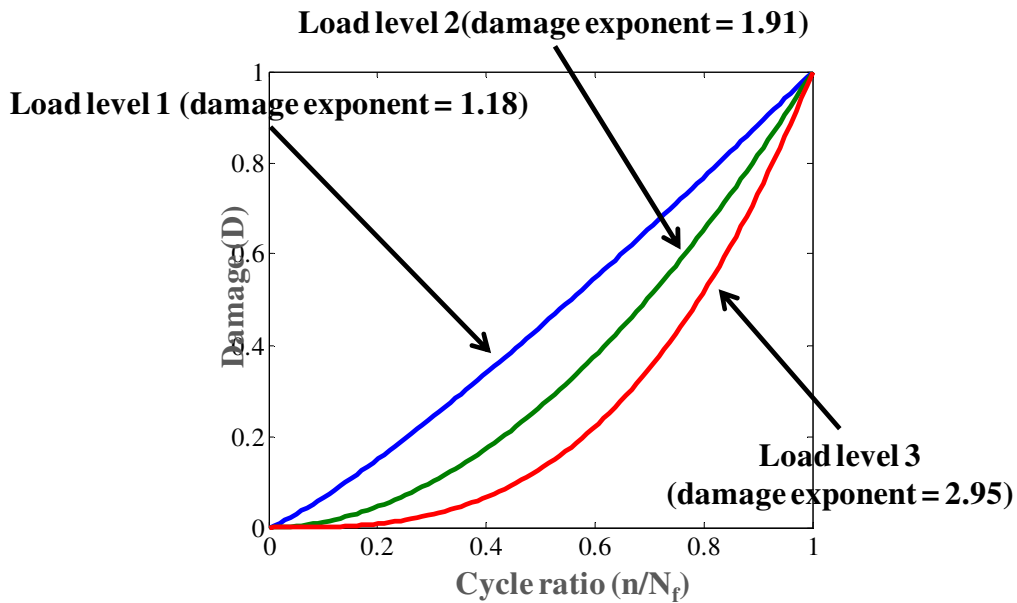


Figure 59. Damage exponents with a failure criterion of 70% load drop

Table XVI. Sensitivity of percentage load drop on the developed damage exponents

% load drop	Damage exponents		
	Load level 1	Load level 2	Load level 3
70%	1.18	1.91	2.95
80%	1.05	1.76	2.69

Bibliography

- [1] Ganesan, S. and Pecht, M., “Lead-free electronics”, Hoboken, New Jersey, John Wiley and Sons, 2006.
- [2] Abtew, M., and Selvaduray, G., “Lead-free solders in microelectronics”, *Materials Science and Engineering: R: Reports*, Vol. 27, No. 5-6, pp. 95-141, 1 June, 2000.
- [3] Osterman, M. and Dasgupta, A., “Life expectancies of Pb-free SAC solder interconnects in electronic hardware”, *Journal of Materials Science: Materials in Electronics*, Vol. 18, No. 1, pp. 229-236, September, 2006.
- [4] Clech, J., “Lead-free and mixed assembly solder joint reliability trends”, *Proceedings of IPC/SMEMA Council APEX Conference*, Anaheim, CA, Vol. 28, No. 3, pp. 1-14, 23-26 February, 2004.
- [5] Huang, M. and Lee, C., “Board level reliability of lead-free designs of BGAs, CSPs, QFPs and TSOPs”, *Soldering and Surface Mount Technology*, Vol. 20, No. 3, pp. 18-25, 2008.
- [6] Pang, J. and Che, F-X., “Isothermal cyclic bend fatigue test method for lead-free solder joints”, *Journal of Electronic Packaging*, Vol. 129, No. 4, pp. 496-503, December, 2007.

- [7] Zhou, Y., Al-Bassyiouni, M., and Dasgupta, A., "Vibration durability assessment of Sn3.0Ag0.5Cu and Sn37Pb solders under harmonic excitation", IEEE Transactions on Components and Packaging Technologies, Vol. 33, No. 2, pp. 319-328, June, 2010.
- [8] Varghese, J. and Dasgupta, A., "Test methodology for durability estimation of surface mount interconnects under drop testing conditions", Microelectronics Reliability, Vol. 47, No. 1, pp. 93-107, January, 2007.
- [9] Palmgren, A., "Die lebensdauer von kugellagern", Veifahrenstechnik, Berlin, Vol. 68, pp. 339-341, 1924.
- [10] Miner, M., "Cumulative damage in fatigue", Journal of Applied Mechanics, Vol. 67, pp. AI59-AI64, 1945.
- [11] Barker, D., Vodzak, J., Dasgupta, A., and Pecht, M., "PWB solder joint life calculations under thermal and vibrational loading", Journal of Institute of Environmental Sciences, Vol. 35, No. 1, pp. 17-25, February, 1992.
- [12] Upadhyayula, K. and Dasgupta, A., "An incremental damage superposition approach for reliability of electronic interconnects under combined accelerated stresses", Proceedings of the ASME International Mechanical Engineering Congress and Exposition, Dallas, Texas, 16-21 November, 1997.
- [13] Qi, H., Osterman, M., and Pecht, M., "Modeling of combined temperature cycling and vibration loading on PBGA solder joints using an incremental

- damage superposition approach”, IEEE Transactions on Advanced Packaging, Vol. 31, No. 3, pp. 463-472, August, 2008.
- [14] Yang, Q, Shi, X., Wang, Z., and Shi, Z., “Finite-element analysis of a PBGA assembly under isothermal/mechanical twisting loading”, Finite Elements in Analysis and Design, Vol. 39, No. 9, pp. 819-833, June, 2003.
- [15] Chen, Y., Wang; C., and Shiah, A., “The experimental study for the solder joint reliability of high I/O FCBGAs with thermal loaded bend test,” IEEE Transactions on Components and Packaging Technologies, Vol. 29, No. 1, pp. 198-203, March, 2006.
- [16] Torres-Montoya, B., Duffek, D., Mason, J., Corona, E., Chengalva, M., and Cavanaugh, M., “Effects of combined cyclic thermal and mechanical loading on fatigue of solder joints,” 9th Intersociety Conference on Thermal and Thermomechanical Phenomena in Electronic Systems, Vol.2, pp. 280-286, 1-4 June, 2004.
- [17] Wong, E., Seah, S., van Driel, W., Caers, J., Owens, N., and Lai, Y.-S., “Advances in the drop-impact reliability of solder joints for mobile applications”, Microelectronics Reliability, Vol. 49, No. 2, pp. 139-149, February, 2009.
- [18] Yang, L., Raghavan, V., Roggeman, B., Yin, L., and Borgesen, P., “On the complete breakdown of miner's rule for lead free BGA Joints”, Proceedings of SMTA International, pp. 152-159, October, 2009.

- [19] Perkins, A. and Sitaraman, S., “A study into the sequencing of thermal cycling and vibration tests”, 58th Electronic Components and Technology Conference, pp. 584-592, 27-30 May, 2008.
- [20] Ladani, L. and Dasgupta, A., “A meso-scale damage evolution model for cyclic fatigue of viscoplastic materials”, International Journal of Fatigue, Vol. 31, No. 4, pp. 703-711, April, 2009.
- [21] Wen, S., Keer, L., and Mavoori, H., “Constitutive and damage model for lead-free solder”, Journal of Electronic Materials, Vol. 30, No. 9, pp. 1190-1196, 2001.
- [22] Xiao, H., Li, X., Liu, N., and Yan, Y., “A damage model for SnAgCu solder under thermal cycling”, 12th International Conference on Electronic Packaging Technology and High Density Packaging, pp. 1-5, 8-11 August, 2011.
- [23] Lall, P., Harsha, M., Suhling, J., Goebel, K., and Jones, J., “Accrued damage and remaining life in field extracted assemblies under sequential thermomechanical loads”, Proceedings of the ASME International Mechanical Engineering Congress & Exposition, Denver, Colorado, 11-17 November, 2011.
- [24] Catelani, M. and Scarano, V. L., “SAC soldering material: A proposal of a new multi-stress accelerated life model”, IEEE SDEMPED International Symposium, pp. 420-425, 2011.

- [25] Richart, F. and Newmark, N., "A hypothesis for the determination of cumulative damage in fatigue", Proceedings of American Society for Testing and Materials, Vol. 48, pp. 767-800, 1948.
- [26] Marco, S. and Starkey, W., "A concept of fatigue damage", Transactions of the ASME, Vol. 76, pp. 627-632, 1954.
- [27] Manson, S.S. and Halford, G.R., "Practical implementation of the double linear damage rule and damage curve approach for treating cumulative fatigue damage", International Journal of Fracture, Vo. 17, No. 2, pp. 169–195, 1981.
- [28] Haswell, P.H., "Durability assessment and microstructural observations of selected solder alloys", Ph.D. Dissertation in Mechanical Engineering, Ph.D. Dissertation. 2001, College Park, MD USA: University of Maryland.
- [29] Mukherjee, S. and Dasgupta, A., "An evaluation of a modified Iosipescu specimen for measurement of elastic-plastic properties of solder materials," IMECE2010-39309, Proceedings of the ASME 2010 International Mechanical Engineering Congress & Exposition, British Columbia, Canada, 2010.
- [30] Zhou, Y., "Harmonic and random vibration durability investigation for SAC305 (Sn3. 0Ag0. 5Cu) solder joint", PhD Dissertation, University of Maryland, College Park, 2009.
- [31] Paris, P.C., Erdogan F., "A critical analysis of crack propagation laws", Journal of Basic Engineering, Series 85D, pp. 528–534, 1963.

- [32] Benachour, M., Hadjoui, A., Benguediab, M., Benachour, N., "Effect of the amplitude loading on fatigue crack growth," *Procedia Engineering*, Vol. 2, No. 1, pp. 121-127, April, 2010.
- [33] Stolkarts, V., Keer, L., and Fine, M., "Damage evolution governed by microcrack nucleation with application to the fatigue of 63Sn-37Pb solder", *Journal of the Mechanics and Physics of Solids*, Vol. 47, No. 12, pp. 2451-2468, December, 1999.
- [34] Shang, J., Zeng, Q., Zhang, L., and Zhu, Q., "Mechanical fatigue of Sn-rich Pb-free solder alloys", *Journal of Materials Science: Materials in Electronics*, Vol. 18, No. 1, pp. 211-227, 2007.
- [35] Cuddalorepatta, G. and Dasgupta, A., "Effect of cyclic fatigue damage accumulation on the elastic-plastic properties of SAC305 solders", 10th International Conference on Thermal, Mechanical and Multi-Physics simulation and Experiments in Microelectronics and Microsystems, pp.1-7, 26-29 April, 2009.